An adaptive robust framework for the optimization of the resilience of interdependent infrastructures under natural hazards

Yiping Fang, Enrico Zio

Manuscript submitted to European Journal of Operational Research

An Adaptive Robust Framework for the Optimization of the Resilience of Interdependent Infrastructures under Natural Hazards

Yiping Fang[1] and Enrico Zio[1, 2]

[1]Chaire Systems Science and the Energy Challenge, Fondation Electricité de France (EDF), Laboratoire Génie Industriel, CentraleSupélec, Université Paris-Saclay, 3 Rue Joliot Curie, 91190 Gif-sur-Yvette, France

[2]Energy Department, Politecnico di Milano, Via La Masa 34, Milano, 20156, Italy

Abstract

This paper proposes a novel adaptive robust optimization (ARO)-based mathematical framework for resilience enhancement of interdependent critical infrastructure (CI) systems against natural hazards (NHs). In this framework, the potential impacts of a specific NH on an infrastructure are firstly evaluated, in terms of failure and recovery probabilities of system components; these are, then, fed into a two-stage ARO model to determine the optimal planning of resilience strategies under limited investment budget, anticipating the most-likely worst realization of the uncertainty of component failures under the NH. For its exact solution, a decomposition method based on simultaneous column-and-row generation (C&RG) is adopted. The approach is applied to a case study concerning the resilience of interdependent power and gas networks (IPGNs) subject to (simulated) wind storms. The numerical results demonstrate the effectiveness of the proposed framework for the optimization of the resilience of interdependent CIs under hazardous events; this provides a valuable tool for making informed pre-hazard preparation decisions. The value of a coordinated pre-hazard planning that takes into account CI interdependencies is also highlighted.

Keywords: risk management; interdependent infrastructure resilience; natural hazard; robust optimization; trilevel programming

1. Introduction

Critical infrastructure (CI) systems such as the electrical power grid, transportation network, Internet, water distribution network, etc. are highly interconnected and mutually dependent, either physically, or geographically, or logically, or through a host of information and communications technologies (so-called "cyber-based systems")(Rinaldi, Peerenboom et al. 2001, Kröger and Zio 2011, Zio 2016). The interdependencies among CI systems serve to their functions, but may also generate new vulnerabilities by creating new hazards and opening new paths for the propagation of failures from one individual CI system to another, resulting in inter-systems cascading failures (Buldyrev, Parshani et al. 2009, Fang, Pedroni et al. 2015). This aspect of CI interdependency has shown in recent disasters, ranging from large-scale power outages to terrorist attacks and windstorms (Vespignani 2010, Zio and Sansavini 2011).

Recent years have seen many disruptions of CIs operation caused by natural disasters (i.e., floods, ice and wind storms, hurricanes, tsunamis, and earthquakes), with substantial impact on the human livelihoods and economic properties (Montz, Tobin et al. 2017). In the USA, for example, the annual impact of weather-related power blackouts ranges from $20 to $55 billion (Campbell 2012) and the trend of such events shows that their frequency has increased over the last 30 years, with a dramatic increase in the 2000s (Panteli and Mancarella 2015). Also, there is a justified concern that the number and severity of these extreme weather events will increase in the future as a result of global warming and climate changes (Cutter, Ismail-Zadeh et al. 2015). This calls for techniques and tools capable of assessing the risk from natural hazards (NHs) on interdependent CIs, in support to policymakers and decision makers for investments in CI protection and resilience measure.

By recognizing the significance of these issues, many governments and organizations have initiated plans and activities for improving the protection and resilience of national/regional interdependent CIs, such as the national CI security and resilience research and development plan in USA (Presidential Policy Directive 2013), the infrastructure resilience programme in UK (Department for Environment 2011), the Australian government's CI resilience strategy and implementation program (Australian Government 2010), and the European Programme for Critical Infrastructure Protection (EPCIP) of the European Commission (Commission of the European Communities 2006). These plans and activities are supported and guided by substantial research efforts in the field, whereby, the number of papers on interdependent CI protection and

resilience has increased exponentially during the past decades (Ouyang 2014, Sharkey, Cavdaroglu et al. 2015).

As a technical concept, resilience is essentially related to the capability of a system to withstand, adapt to and quickly recover from the effects of a disruptive event (Fang, Pedroni et al. 2016, Hosseini, Barker et al. 2016, Zio 2016). For its quantitative evaluation, a number of resilience metrics have been proposed, most of them based on the system performance curve under disruption (Hosseini, Barker et al. 2016) and describing numerically the two factors of *system robustness* and *recovery rapidity* defined by Bruneau, Chang et al. (2003). *System robustness* is quantified by the system functionality level immediately after the event; *recovery rapidity* quantifies how quickly the system recovers after the event. Enhancements of system resilience prior to disruption can be achieved by allocating resources for interventions that reduce the value of one or both of the two above mentioned factors that characterize resilience (He and Zhuang 2016, MacKenzie and Zobel 2016).

In the present paper, we focus on the pre-disruption investment planning for enhancing the resilience of interdependent CI systems against NHs. In the literature, a range of approaches have been proposed for the assessment and optimization of CI resilience under NHs, though mostly for single CI systems. A probabilistic framework composed of four coupled models has been proposed by Ouyang and Dueñas-Osorio (2014) for quantifying the resilience of electric power systems under hurricanes. Similar multi-phase resilience assessment approaches have been applied to analyze the impact of windstorms and floods on Great Britain's power transmission system (Panteli and Mancarella 2015, Espinoza, Panteli et al. 2016, Panteli, Pickering et al. 2017). Franchin and Cavalieri (2015) proposed a simulation-based probabilistic assessment framework for quantifying the resilience of CI systems under earthquakes. The seismic resilience of coupled municipal water system and electrical power system are analyzed by Adachi and Ellingwood (2008) using a probability-based simulation method. Rocchetta, Li et al. (2015) developed a probabilistic risk assessment and risk-cost optimization framework for distributed power generation systems considering the effects of extreme weather conditions (i.e., lightening and strong wind).

The above resilience studies analyze different single CI systems under different types of NHs, typically within a probabilistic simulation framework. This approach is valuable for assessing system resilience in a statistical manner, e.g., computing the average system performance loss or identifying the critical components, based on different realizations of specific hazards. However, for a specific realization/estimation of a hazard event, the uncertainty within the estimated failure probabilities might be propagated by the simulation-based

methods, leading to underestimation or overestimation of system vulnerability. Actually, it is very difficult to predict accurately the failure probability of each component in a CI system exposed to a specific NH, like a hurricane or earthquake (Pidgeon 2012). More robust tools to assist decision makers during pre-hazard preparation are needed (Fang, Sansavini et al. 2017).

System resilience optimization is concerned with the development of strategies to mitigate the performance loss of a system under disruption (i.e., increase the *system robustness*) and/or to restore a system to normal operations as quickly and efficiently as possible, following disruption (i.e., enhance system *recovery rapidity*). For quickly restoring post-disruption service of interdependent CI systems, a network flows-based mixed integer programming (MIP) model has been proposed by Lee II, Mitchell et al. (2007). With this model, the impact of interdependencies between the supply chain network (SCN) and its supporting infrastructures on the SCN's recovery from a disruption (Gong, Mitchell et al. 2014), and the value of information-sharing for interdependent network restoration (Sharkey, Cavdaroglu et al. 2015) have been studied. Nurre, Cavdaroglu et al. (2012) extended this network flow-based model by integrating the scheduling decisions into the CI system restoration, arriving at an integer programming formulation of the integrated network design and scheduling problem. Zhang, Liu et al. (2016) formulated a two-stage MIP for resource allocation in interdependent CI systems with a focus on minimizing the restoration time. All of the above-mentioned models concern post-disruption decision-making, assuming that a disruption has already happened.

In the context of pre-disruption decision-making for CI resilience improvement, the problem is usually formulated as multi-level defender-attacker optimization models, whose general framework is introduced in Brown, Carlyle et al. (2006). In this framework, there is a virtual attacker who seeks to find the most harmful attack strategy to disrupt the system and a defender who pursues minimum damage from the attack through the pre-attack defense and post-attack response. The interactions between the attacker and the defender can be modeled by a tri-level defender-attacker-defender (DAD) game, which also takes the form of two-stage adaptive robust optimization (ARO) (Bertsimas, Brown et al. 2011, Ruiz and Conejo 2015). It is noted that albeit the two-stage ARO and the DAD game model have different origins, they share an identical tri-level optimization structure. This modeling framework has been applied to identify the optimum resilience strategies for electric power grids (Alguacil, Delgadillo et al. 2014, Yuan, Wang et al. 2016, Fang and Sansavini 2017), rail systems (Alderson, Brown et al. 2011), commodity distribution networks (Alderson, Brown et al. 2015), facility networks (Losada, Scaparra et al. 2012), general CIs (Scaparra and Church 2008) and interdependent CIs (Ouyang 2017). By assuming an intelligent attacker and exploiting its optimization,

these multi-level defender-attacker models intend to estimate a worst case damage scenario for any feasible protection strategy. For the pre-disruption investment planning of interdependent CIs under NHs, however, the pure worst-case-oriented ARO (i.e., DAD) approaches may be overly conservative. Actually, future projections of specific NH events are usually available via climate models (Davis, Wang et al. 2008, Holland, Belanger et al. 2010, Batke, Jocque et al. 2014), though usually associated with uncertainties. Without taking into account the projection information of specific NHs as well as the spatiotemporal correlations of the NHs which strongly impact the probabilities of some common cause failures, the pure worst-case-oriented ARO approaches might overestimate the system functionality loss and lead to inefficient or even misleading protection decisions.

To overcome the drawbacks of the aforementioned methods, this paper presents a novel ARO-based mathematical framework for enhancing the resilience of interdependent CI systems against NHs by integrating the projected information of specific NHs. In particular, the time-varying failure probabilities of system components are firstly computed by integrating the spatial-temporal profile of the NHs and the structural fragilities of the components. The restoration time of components is also estimated probabilistically. Then, the information about the probabilities of failure and restoration of the components is fed to the virtual attacker in the ARO as a constraint for its attack decisions. Therefore, the failure scenarios identified by the optimization represent the *most-likely* worst cases under the specific hazard. The proposed approach bridges the gap between the difficulties of accurately predicting the hazard information in the classical probability-based analyses and the over-conservativeness of the pure worst-case-oriented ARO models for CI resilience under a specific NH, thus, providing a useful tool to for making informed pre-hazard preparation decisions.

The remainder of this paper is organized as follows. Section 2 introduces the models for evaluating the impacts of NHs on individual CIs, including threat characterization, structural fragility, and component restoration time models. In Section 3, the detailed formulation of the optimization framework for the resilience of interdependent CIs is proposed. Section 4 proposes the solution methodology for the proposed optimization model. Section 5 presents the numerical results by applying the proposed framework to the interdependent power and gas test systems. Concluding remarks are provided in Section 6.

2. Impact of NHs on CIs

Depending on the nature of the formation process, NHs can be categorized into: geophysical (earthquake, volcano and tsunami), meteorological (tropical storm, tornado, blizzard, ice storm, and drought), hydrological (flood), biological (epidemics and insect pests) and extraterrestrial (meteor). The former three types are usually most destructive to CI systems. They include not just one single instantaneous impact, but multiple and even continuous impacts. For instance, the windstorms that affected China in 2005 caused more than 60 high-voltage power transmission towers to collapse, and the ice and snow storms that devastated a large area in South China lasted for hours (Xie and Zhu 2011). Disasters can even last for days, like the hurricane Irma (2017) in the Caribbean and the United States, where many of the CIs were wiped out in most of the Caribbean islands and the eastern US (especially Florida). Moreover, hazard impacts often are difficult to characterize because a given NH may initiate a number of different threats. For example, tropical storms can cause damages through wind, rain, storm surge and islanding flooding. The most significant characteristics for assessing the disaster impacts are speed, onset, availability of perceptual cues (such as wind, rain, or ground movement), intensity, scope and duration of impact (Lindell and Prater 2003). Table 1 summarizes the basic characteristics of different types of NHs (Wang, Chen et al. 2016, Fang, Sansavini et al. 2017).

Table 1. Characteristics of different NHs

Disaster type	Impact region	Predictability	Span/Area	Affecting time
Tropical storm hurricane	Coastal regions	24-72 hours, moderate to good	Large (radius up to 1500km)	Hours to days
Tornado	Inland plains	0-2 hours, bad to moderate	Small (radius up to 8km)	Minutes to hours
Blizzard, ice storm	High latitude regions	24-72 hours, moderate to good	Large (up to 1500 km)	Hours to days
Earthquake	Regions on fault lines	Seconds to minutes, bad	Small to large	Minutes to days (aftershock)
Tsunami	Coastal regions	Minutes to hours, moderate	Small to large	Minutes to hours
Drought, Wild fire	Inland regions	Days, good	Medium to large	Days to months
Flooding	Low-lying regions	Moderate to good	Small to large	Days to months

The physical impacts of NHs on CIs vary substantially across different NH types and CI systems. The prediction and evaluation of such impacts are challenging tasks due to the uncertainty in the highly dynamic evolution of the hazards themselves and the inherent complexity of the large-scale CI systems. A framework for quantifying the physical impacts of NHs on CIs is illustrated in Figure 1 (Ouyang and Dueñas-Osorio 2014, Panteli and Mancarella 2015). The core of the framework consists of 1) threat characterization model, which associates the NH parameters with the estimation of the local environment for the CI system components; 2) structural fragility model, which determines the functional states of the CI system components; 3) component restoration model, which estimates the restoration times of the impacted components. The inputs of the framework are the parameters characterizing the NHs, e.g., taken from weather information, and the evaluation by the combination of the three models provides in outputs the spatiotemporal profile of the functional states of the CI components under the NHs.

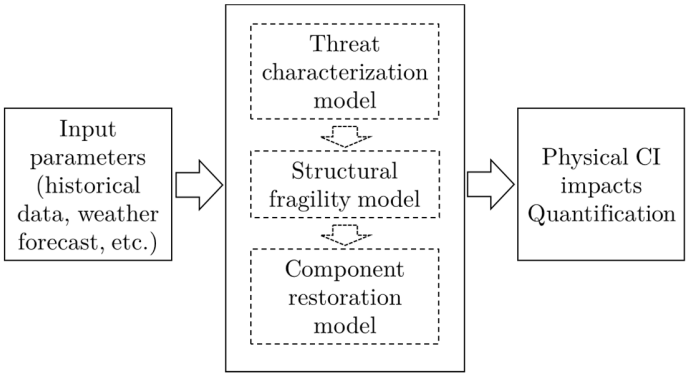

Figure 1. A general framework for quantifying the physical impacts of NHs on CIs

In the remaining part of this section, we introduce how the impacts of a specific type of NH, i.e., wind storms (typhoon, cyclone or hurricane), on components of electrical power systems can be analyzed through the combination of threat characterization, fragility models of system components and system restoration models.

2.1. Threat characterization

The primary step to evaluate the impacts of NH on a CI system is to model the spatiotemporal profile of the threats associated to the hazard, given that CI systems (like power grids) cover extensive geographic scales (Panteli and Mancarella 2015, Zio 2016). Threat characterization models aim to associate the hazard parameters with the local threat intensity for each CI component.

We take windstorm as an example, which is represented by forecasted data, like landing time and position, approaching angle, translational velocity, central pressure difference, maximum wind speed, radius of maximum wind, as obtained by climate models (CMs) and real measurement data (Davis, Wang et al. 2008). The majority of windstorm-related power outages in power transmission occurs because high intense winds directly blow down poles, and/or trees are blown over power lines and poles (Han, Guikema et al. 2009). Hence, the intensity of wind is a characteristic of the primary threat of storms.

The wind speeds profile of a storm can be generated through parametric radial wind field models (Davis, Wang et al. 2008, Holland, Belanger et al. 2010, Batke, Jocque et al. 2014). The wind speed at location (x, y) at time t can be represented by Holland, Belanger et al. (2010)

$$v(x, y; t) = v_m \left\{ \left(\frac{R_m}{r} \right)^b e^{\left[1 - \left(\frac{R_m}{r} \right)^b \right]} \right\}^a \tag{1}$$

where r is the distance from the point to the storm center $\left(x_{center}(t), y_{center}(t)\right)$, which moves with the translational velocity v_t of the storm, v_m is the maximum wind speed, R_m is the radius of maximum wind (also called wind radius) and can be calculated from the storm eye-diameter (ED) (Batke, Jocque et al. 2014), b is the empirical Holland parameter and can be estimated based on the central pressure of the storm, and a is a scaling parameter that adjusts the wind profile shape and a value of $a = 0.5$ is typically used (Holland, Belanger et al. 2010). Figure 2 shows an example of wind profile of the Typhoon Meranti at 2016 September 14, 18:00 (GMT+8) when making landfall at Xiamen, China, calculated by Eq. (1) based on the dataset from the National Oceanic and Atmospheric Administration (NOAA) of the United States (NOAA 2016).

Structural damage from windstorms is mostly related to peak gust wind speed, which is the largest speed during a specified period (usually 3 seconds). A gust factor can be used to convert the surface wind speed calculated by Eq. (1) to the most likely peak gust speed. A gust model has been developed for modeling gust factors, and a justified empirical value of 1.287 can be used (Vickery and Skerlj 2005).

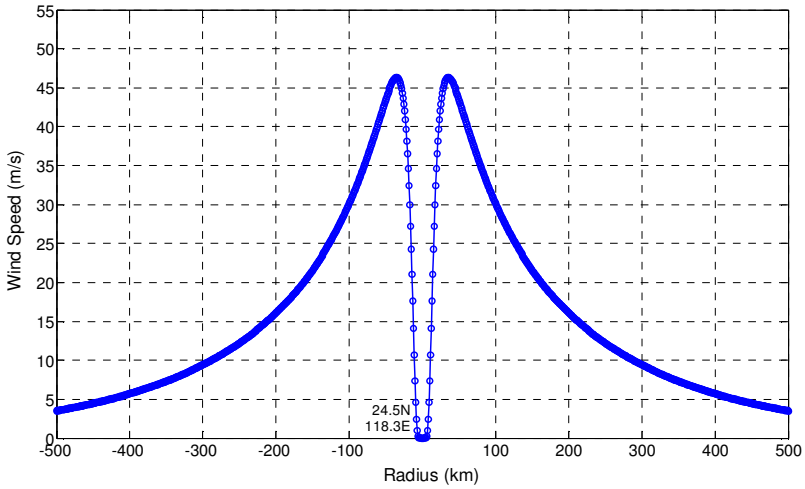

Figure 2. Wind profile of the Typhoon Meranti at 2016 September 14, 18:00 (GMT+8) when making landfall at Xiamen, China

Storm-induced flooding is not considered here as a major threat to power systems, though storm surges associated with landfalling windstorms can cause damages to underground power components and substations (Brown 2009). Yet, detailed threat models of storm flooding considering local geospatial information exist in the literature (Lin, Emanuel et al. 2012, Aerts, Lin et al. 2013) and they can be included if relevant data are available.

2.2. Structural fragility models

The functional state of the components of a CI system can be determined by the following three steps: i) identify the key (types of) components of the system, ii) model their fragility, and iii) estimate their failure probability.

In the first step, the types of components identified as vulnerable to the threat and whose failures could possibly have a high impact on system performance, are identified. Although power systems comprise many types of components, it is practical to mainly focus on the most important ones, e.g. substations and overhead lines (including support structures and the conductors between structures). In this study, we assume that generation is not directly affected by the windstorm (with the exception of wind generation), albeit generation nodes can be disconnected due to outages of transmission corridors.

Fragility analysis is required to compute the probability of failure of components exposed to given levels of threat intensity. The concept of *fragility curves* originates from structural reliability analysis (Li and

Ellingwood 2006, Panteli and Mancarella 2015) and represents the conditional probability of failure of a structural element as a function of disaster strength parameters like wind speed and precipitation.

The calculation of fragility curves is often based on parametric statistical models, taking into account factors like the design strength and aging. For different CI components, different fragility curves may best fit to historical data. For power systems, there is a range of literature discussing the structural fragility models subject to wind loading (Savory, Parke et al. 2001, Hangan, Savory et al. 2008, Bjarnadottir, Li et al. 2012, Salman, Li et al. 2015). The lognormal distribution is usually assumed to describe the fragility curves of support poles and overhead power lines (Bjarnadottir, Li et al. 2012, Salman, Li et al. 2015); the direct threat-induced failure probability $p\big(v(t)\big)$ as a function of the wind speed $v(t)$ is given by the following lognormal cumulative distribution function (CDF)

$$p\big(v(t)\big) = \Phi\left[\frac{\ln(v(t)/m)}{\sigma}\right] \tag{2}$$

where $\Phi(\cdot)$ is the CDF of the standard normal distribution, m is the median of the fragility function and σ is the logarithmic standard deviation of the intensity measurement. The values of the parameters m and σ are related with the structural characteristics of the component under consideration.

In the third step, the overall failure probability of each component is computed by taking into account direct and indirect threats that could lead to failure. For example, besides failures caused by direct wind load, overhead power lines also fail due to falling trees and flying debris. Actually, around 55.2% of power outages in the U.S. Northeast regional distribution systems are caused by trees falling down during wind storms (Li, Zhang et al. 2014). In addition, overhead lines consist of support poles, conductor wires and other types of equipment. The collapse of a single pole or conductor results in the disconnection of the entire line. Therefore, the overall failure probability of an overhead line is modeled as a series system with the fragility analysis of each pole and conductor associated with that line. It is assumed that the fragility of different components of an overhead line is independent. The overall failure probability of an overhead line l under wind speed $v(t)$ is calculated as (Ouyang and Dueñas-Osorio 2014)

$$p_{l,failure}\big(v(t)\big) = 1 - \prod_{k=1}^{m}\big[1 - p_{S_k}\big(v(t)\big)\big]\prod_{k=1}^{n}\big[1 - p_{C_k}\big(v(t)\big)\big] \tag{3}$$

where m is the number of poles supporting line l, n is the number of conductor lines between two adjacent poles at line l, p_{S_k} is the conditional failure probability of the kth pole at line l which can be given by Eq.

(2) and p_{C_k} is defined as the failure probability of conductor k between two poles: this probability can be modeled by (Ouyang and Dueñas-Osorio 2014)

$$p_{C_k}(v(t)) = \max\left(p_{C_k,w}(v(t)), \varpi p_{C_k,wt}(v(t))\right) \tag{4}$$

where $p_{C_k,w}(v(t))$ is the direct wind-induced failure probability of conductor k, $p_{C_k,wt}(v(t))$ represents the fallen tree-induced failure probability of conductor k and ϖ is the average tree-induced failure probability of overhead conductors, reflecting the efforts of trimming trees by utilities and assumed constant (Ouyang and Dueñas-Osorio 2014). The direct wind-induced failure probability $p_{C_k,w}(v(t))$ can be computed by Eq. (2), based on the structure property parameters of the conductor (Bayliss, Bayliss et al. 2012). The fallen tree-induced failure probability $p_{C_k,wt}(v(t))$ can be calculated approximately by empirical models such as the one proposed by Canham, Papaik et al. (2001). For simplicity, in this study we do not consider the tree-induced failure probability of overhead conductors.

2.3. Component restoration time model

A range of models have been proposed in the literature for the post-disaster restoration processes of various CI systems (Liu, Davidson et al. 2007, Nateghi, Guikema et al. 2011, Duffey and Ha 2013). The output of these models is usually represented by restoration curves at the system level (percentage of customers with service versus time) or by system average interruption duration indices (SAIDI). Yet, for system criticality analyses aiming at supporting pre-event decision making, models for estimating the restoration times of components are required. The response to the disaster and the restoration time of failed CI components varies directly with: (i) storm categories, (ii) locations and types of damaged components and (iii) the amounts of repair crews and material resources available. Thus, the restoration time of a failed component can be expressed by

$$T = f(category, location, type, resources). \tag{5}$$

In practice, it is usually challenging to have an analytic form of $f(\cdot)$. Instead, probabilistic models like Gaussian (Ouyang and Dueñas-Osorio 2014) and exponential distributions (Zapata, Silva et al. 2008, Espinoza, Panteli et al. 2016) are traditionally used to represent the repair processes of power system components. Zapata, Silva et al. (2008) studied realistic historical data and showed that the lognormal distribution is a more appropriate model for component repair times in power systems. On the other hand, storm categories and intensities significantly affect the repair times of the damaged components, e.g., more

time is needed for the repair crews to approach safely the affected areas under severe weather conditions. This effect can be modeled as an increase in the Mean Time To Repair ($MTTR$) of components by a factor of restoration stress (RS). For example, Espinoza, Panteli et al. (2016) assumed random RS values in the range $\{2, 4\}$ for overhead lines restoration under moderate storms. In practice, data about RS can be obtained or estimated from past repair experience under different storm categories (Bhuiyan and Allan 1994).

Therefore, for a given storm category, the probability that a failed component, e.g., an overhead line l, is repaired within time T is given by

$$p_{l,repair}(\tau \leq T|catg) = \Phi\left\{\frac{\ln[T/(RS_{catg} \cdot MTTR_l)]}{\sigma}\right\} \tag{6}$$

where RS_{catg} represents the restoration stress under storm category $catg$, $MTTR_l$ is the $MTTR$ of overhead line l under normal operation and σ is the logarithmic standard deviation of restoration time.

3. Mathematical formulation of the optimization model

In this section, the detailed mathematical formulation of the proposed robust optimization framework for the resilience of interdependent CIs under NHs is provided.

A network flow-based approach is used in this study for the modeling of interdependent CIs, where each CI is modeled as a network and their interdependencies are represented via inter-links. Specifically, the set of CIs of concern is denoted by $\boldsymbol{\kappa}$. Each CI k in $\boldsymbol{\kappa}$ is modeled by a network $G^k(V^k, L^k)$ described by a collection of nodes V^k and edges L^k. Each link $l \in L^k$ in CI network k has an associated capacity $\bar{f}_l^k$ representing the maximal amount of flow that can pass through it, while each node $n \in V^k$ has a supply capacity $\bar{g}_n^k$ and a required demand $\hat{d}_{nt}^k$ of flow for its nominal operation at time t. Flow distributes through the CI network according to the flow capacities of the links and supply capacities of the nodes, following the rule of flow conservation.

For CI network $k \in \boldsymbol{\kappa}$, its resilience to a NH is regarded as the cumulative system performance level during the NH, quantified by the normalized total satisfied demand level

$$R^k = \frac{\sum_{t\in\mathbb{T}}\sum_{n\in V^k} d_{nt}^k}{\sum_{t\in\mathbb{T}}\sum_{n\in V^k} \hat{d}_{nt}^k} \tag{7}$$

where d_{nt}^k denotes the satisfied flow at node $n \in V^k$ at time t, and $\mathbb{T}$ is the set of all discrete times within the hazard horizon. Then, the resilience of the interdependent CIs under this event is represented by the weighted sum of the resilience of each CI network, expressed by

$$R = \sum_{k \in \boldsymbol{\kappa}} w^k \frac{\sum_{t \in \mathbb{T}} \sum_{n \in V^k} d_{nt}^k}{\sum_{t \in \mathbb{T}} \sum_{n \in V^k} \hat{d}_{nt}^k} \tag{8}$$

where w^k is the weighting factor for the resilience of CI network k.

For the resilience of interdependent CIs under a NH, our purpose is to find the optimal planning of resilience strategies under limited investment budget, anticipating the worst possible realization of the uncertainty of component failures under the NH. In particular, a two-stage ARO model is set up as follows:

1) The optimal investment planning, denoted by decision variable $\boldsymbol{x}$, is sought by maximizing the resilience of the interdependent CIs under a limited budget. This is done by anticipating that, right after this decision is made:
2) the NH will behave in the worst possible manner given the forecasted but uncertain information of the NH. Therefore, assuming $\boldsymbol{x}$ is fixed, NH will select the realization of the uncertain component failures, denoted by variable $\boldsymbol{u}$, which minimizes the interdependent CIs resilience; this is done by anticipating that, right after the worst uncertainty outcome is realized:
3) the interdependent CIs will try to adapt to it via response operations; thus, assuming that $\boldsymbol{x}$ and $\boldsymbol{u}$ are fixed, the system operators will select the optimal operation, denoted by decision variables $\boldsymbol{o}$, in order to maximize the systems' resilience.

For illustrative purposes, this paper considers two typical ex-ante resilience strategies, i.e., protecting transmission lines and placing distributed generation (DG) units, which have been considered also by other scholars in the literature (Yuan, Wang et al. 2016). In this study, protected lines are assumed to be invulnerable and cannot be damaged by NHs. Also, the DG units are used for generation backup in case of supply interruption under NHs and can continue supplying power to connected loads. Other possible resilience strategies can be easily incorporated into our analysis framework. Since the most common components disrupted under NHs are transmission lines in electrical power grids (Wang, Chen et al. 2016), this study focuses on outages of transmission lines. But, the approach can be extended to account for the outages of other components. The transmission lines damaged by the NHs are assumed to be completely unusable until they are repaired.

The two-stage ARO framework for the optimal investment planning of interdependent CIs under NHs is framed within a three-level max-min-max problem, which takes the form of defender-attacker-defender game models (Brown, Carlyle et al. 2006, Alderson, Brown et al. 2011, Fang and Sansavini 2017, Ouyang and Fang 2017). It is noted that even the defender-attacker-defender game model and the two-stage ARO have different origins, they share an identical tri-level optimization structure.

The proposed two-stage ARO model uses the following notations:

Indices, sets, and parameters

Input parameters for each network

$k \in \boldsymbol{\kappa}$	Set of all energy networks; $k = 1$ represents the power network
$l \in L^k$	Set of transmission lines in network k
$n \in V^k$	Set of nodes in network k
$o(l)$	Origin or sending node of line l
$r(l)$	Destination or receiving node of line l
$L_n^{k,nbr}$	Set of neighboring lines of node $n \in V^k$, i.e., $L_n^{k,nbr} = \{l \vert l \in L^k : o(l) = n \text{ or } r(l) = n\}$
$\bar{g}_n^k$	Capacity of generation at node $n \in V^k$
$\bar{g}_n^{k,D}$	Capacity of distributed generation at node $n \in V^k$
$\bar{f}_l^k$	Capacity of line $l \in L^k$
$\hat{d}_{nt}^k$	Demand at node $n \in V^k$ at time t
X_l	Reactance of power transmission line l
θ^{max}	Maximum allowable limit for θ_{nt} variables

Input parameters for interdependencies

$V^{k,C}$	Set of all nodes in network k that depend on the nodes of other networks to operate, i.e., the consequent nodes
$E^{k,C}$	Set of all lines in network k that depend on the nodes of other networks to operate, i.e., the consequent links

$V^{k,A}$ Set of all nodes in network k that any other network nodes depend on, i.e., the antecedent nodes

$V^{k\leftarrow m,C}$ Set of all nodes in network k that depend on the nodes in network $m(m \neq k)$ to operate

$E^{k\leftarrow m,C}$ Set of all lines in network k that depend on the nodes in network $m(m \neq k)$ to operate

$V^{k\rightarrow m,A}$ Set of all nodes in network k that the operation of the nodes in network $m(m \neq k)$ depend on

$F_{i,j}^{k\rightarrow m}$ Set of ordered pairs (i,j) associated with node $i \in V^{k\rightarrow m,A}$ and node $j \in V^{m\leftarrow k,C}$, and node j is operational only when the demand of flow of node i in network k can be fully satisfied

$M_{i,j}^{k\rightarrow m}$ Set of ordered pairs (i,j) associated with node $i \in V^{k\rightarrow m,A}$ and line $j \in E^{m\leftarrow k,C}$, and line j operates with its full capacity when the demand of flow of node i in network k is fully satisfied; otherwise line j operates with a reduced capacity $\tilde{f}_j^m$

Input parameters for interdependent CIs resilience investment

B_P Monetary investment budget for system resilience

$c_l^{k,P}$ Cost of protecting line l in network k

$c_n^{k,D}$ Cost of placing a distributed generation at node $n \in V^k$

Input parameters for NHs

Γ^k Budget of failure uncertainty for network k

Υ^k Budget of recovery uncertainty for network k

$\mathbb{T}$ Set of discrete times of hazards

T^{max} Maximal repair time of failed lines

$\boldsymbol{u} \in \mathbb{U}$ Uncertainty set of component failures

$\boldsymbol{o} \in \mathbb{O}$ Feasible set of system operation under a realization of uncertainty

Decision variables

Ex-ante protection decision variables

x_l^k $x_l^k = 1$ if a line l in network k is protected, 0 otherwise

x_n^k $x_n^k = 1$ if distributed generation is placed at node n in network k, 0 otherwise

Disruption uncertainty variables

v_{lt}^k $v_{lt}^k = 1$ if a line l in network k is damaged to be offline at time t, 0 otherwise

y_{lt}^k $y_{lt}^k = 1$ if a line l in network k is restored to be online within time t, 0 otherwise

z_{lt}^k $z_{lt}^k = 1$ if a line l in network k is online (operational) at time t, 0 otherwise

Ex-post operation decision variables

$\delta_{ijt}^{k\to m}$ Interdependency variable that is equal to 1 if the interdependency from node i in network k to component (node or line) j in network m works normally at time t, 0 otherwise

θ_{nt} Phase angle in node n in the power network ($k = 1$) at time t

f_{lt}^k Flow in line l in network k at time t

g_{nt}^k Flow generated at node $n \in V^k$ at time t

d_{nt}^k Satisfied flow at node $n \in V^k$ at time t

Mathematically, the hierarchical structure of the two-stage ARO is represented by the following tri-level optimization problem:

$$\max_{\boldsymbol{x}} \min_{\boldsymbol{u}\in\mathbb{U}(\boldsymbol{x})} \max_{\boldsymbol{o}\in\mathbb{O}(\boldsymbol{x},\boldsymbol{u})} R(\boldsymbol{x},\boldsymbol{u},\boldsymbol{o}) \tag{9}$$

s.t.

$$\sum_{k\in\boldsymbol{\kappa}} \left(\sum_{l\in L^k} c_l^{k,P} x_l^k + \sum_{n\in V^k} c_n^{k,D} x_n^k \right) \le B_P \tag{10}$$

$$x_l^k, x_n^k \in \{0,1\}\ \forall l, n, k \tag{11}$$

where $R(\boldsymbol{x},\boldsymbol{u},\boldsymbol{o})$ is the objective function representing the resilience of the interdependent CIs under a NH and is calculated by Eq. (8). The first level problem in (9) is to identify the optimal set of transmission lines to protect and the optimal sites to place DG units so that the resilience of the interdependent CIs is maximized. The worst case realization of the uncertainty of the NH's impacts on the systems and the successive adaptive action is considered in the middle-low level problem $\mathcal{H}(\boldsymbol{x}) = \min_{\boldsymbol{u}\in\mathbb{U}(\boldsymbol{x})} \max_{\boldsymbol{o}\in\mathbb{O}(\boldsymbol{x},\boldsymbol{u})} R(\boldsymbol{x},\boldsymbol{u},\boldsymbol{o})$.

Note that $\boldsymbol{u} \in \mathbb{U}(\boldsymbol{x})$ defines the uncertainty set dependent on the severity of NHs and $\boldsymbol{o} \in \mathbb{O}(\boldsymbol{x}, \boldsymbol{u})$ represents the feasible set of system operation under an investment planning $\boldsymbol{x}$ and a realization of uncertainty $\boldsymbol{u}$. Constraint (10) enforces the limit of the total investment budget. Constraint (11) enforces the integrality of the investment decision variables.

The uncertainty set $\mathbb{U}$ of component failures under a hazard is modeled as follows:

$$\mathbb{U}(\boldsymbol{x}) = \left\{ \boldsymbol{u} \left| \sum_{l \in L^k} (-\log_2 p_{lt}^k) v_{lt}^k \leq \Gamma^k, \forall k, t \right. \right. \tag{12}$$

$$\sum_{t \in \mathbb{T}} v_{lt}^k \leq 1 - x_l^k, \forall k, l \tag{13}$$

$$\sum_{l \in L^k} \left[-\log_2 \overline{\boldsymbol{\mathcal{P}}}_{l,repair}(t|catg) \right] y_{lt}^k \leq \Upsilon^k, \forall k, t \in \{1, \ldots, T^{max}\} \tag{14}$$

$$\sum_{t=1}^{T^{max}} y_{lt}^k = \sum_{t \in \mathbb{T}} v_{lt}^k, \forall k, l \tag{15}$$

$$z_{lt}^k + \sum_{\tau = max\left\{t - \sum_{t=1}^{T^{max}} t \cdot y_{lt}^k, 1\right\}}^{t} v_{l\tau}^k = 1, \forall k, l, t \in \mathbb{T} \tag{16}$$

$$\left. v_{lt}^k, y_{lt}^k, z_{lt}^k \in \{0,1\}, \forall k, l, t \right\} \tag{17}$$

where $\boldsymbol{u} = [\boldsymbol{v}, \boldsymbol{y}, \boldsymbol{z}]$ indicates the operation states of the lines in the interdependent CI systems over the whole time horizon of the hazard. Constraint (12) defines the uncertainty budget of system failure. Inspired by Shannon's information theory (Shannon and Weaver 1998), this definition relates the failure probabilities $\boldsymbol{p}$ of the system components and their binary damage variables $\boldsymbol{v}$ at each time period. The parameter Γ^k represents the total uncertainty budget of failure of network k and can be assigned by the analyst. The failure probability p_{lt}^k is calculated by Equation (3). Constraint (12) states that the failure of a "reliable" line, i.e., having smaller failure probability p_{lt}^k, is more "surprising", i.e., takes up more failure uncertainty budget than the failure of a vulnerable line that has a larger failure probability p_{lt}^k. For instance, if the failure probability of a line $p_{lt}^k = 0$, then the occurrence of its failure takes an infinite large failure uncertainty budget and v_{lt}^k will be 0, if Γ^k is not infinite. Conversely, if the failure probability $p_{lt}^k = 1$, then the occurrence of its failure takes zero budget, and v_{lt}^k will be 1 in the optimization. Therefore, given a vector $\boldsymbol{p}$ of the failure probability of the system components, a large Γ^k implies a large failure budget for system k and thus a large upper limit of the number of failed lines. In other words, by setting a large Γ^k the decision maker anticipates a large damage caused by the hazard. Constraint (13) states that a transmission line

cannot fail if it has been protected ($x_l^k = 1$) and it can only fail once during the horizon of the hazard if it has not been protected ($x_l^k = 0$). Similar to the Constraint (12), (14) bounds the uncertainty budget Υ^k for the recovery times of components in network k: a large value of Υ^k represents a high degree of uncertainty with regard to the restoration times of failed lines in network k. In (14), $\overline{\boldsymbol{\mathcal{p}}}_{l,repair}(t|catg)$ represents the normalized probability that a failed line l is recovered within time duration $t(t \leq T^{max})$ under a specific category of hazard, and is calculated as follows

$$\boldsymbol{\mathcal{p}}_{l,repair}(t|catg) = p_{l,repair}(t|catg) - p_{l,repair}(t-1|catg) \tag{18}$$

$$\overline{\boldsymbol{\mathcal{p}}}_{l,repair}(t|catg) = \frac{\boldsymbol{\mathcal{p}}_{l,repair}(t|catg)}{\max\limits_{t\in\{1,\dots,T^{max}\}} \boldsymbol{\mathcal{p}}_{l,repair}(t|catg)} \tag{19}$$

where $p_{l,repair}(t|catg)$ is obtained by Equation (6). It is noted that $\overline{\boldsymbol{\mathcal{p}}}_{l,repair}(t|catg)$ always takes the value of 1 for the time period with the largest probability, i.e., for $t = arg\max \boldsymbol{\mathcal{p}}_{l,repair}(t|catg)$. Constraint (15) indicates that a failed line is repaired within a specific time duration. Constraint (16) imposes that a line is either functional, i.e., $z_{lt}^k = 1$ or failed and not being repaired, i.e., $\sum_{max\{t-\sum_{t=1}^{T^{max}} t\cdot y_{lt}^k, 0\}}^{t} v_{lt}^k = 1$ where $\sum_{t=1}^{T^{max}} t \cdot y_{lt}^k$ gives the repair time of the line. Constraint (17) imposes the integrity conditions for the variables $\boldsymbol{v}, \boldsymbol{y}$ and $\boldsymbol{z}$.

In the third level of (9), the feasible set of system operations under a realization of uncertainty $\boldsymbol{u} \in \mathbb{U}$ for interdependent CIs is formulated based on a network flow-based approach, which is most applicable to single-commodity infrastructures including, for example, power, water, wastewater, gas and supply chain systems (Nurre, Cavdaroglu et al. 2012). It is noted that different physical constraints may be enforced to the network flow depending on the specific types of CI systems of interest (Fang and Sansavini 2017). For illustrative purposes, this paper considers interdependent power and gas networks (IPGNs), combining the linearized DC power flow model for the power network and the general flow-based model for the gas network as follows

$$\mathbb{O}(\boldsymbol{x}, \boldsymbol{u}) = \left\{ \boldsymbol{o} \,\middle|\, g_{nt}^k + \sum_{l\in L^k|r(l)=n} f_{lt}^k - \sum_{l\in L^k|o(l)=n} f_{lt}^k = d_{nt}^k, \forall k, n, t \right. \tag{20}$$

$$0 \leq g_{nt}^k \leq \bar{g}_n^k + x_n^k \bar{g}_n^{k,D}, \forall k, n, t \tag{21}$$

$$0 \leq d_{nt}^k \leq \hat{d}_{nt}^k, \forall k, n, t \tag{22}$$

$$-z_{lt}^{k}\bar{f}_{l}^{k} \leq f_{lt}^{k} \leq z_{lt}^{k}\bar{f}_{l}^{k}, \forall k, l, t \tag{23}$$

$$X_l f_{lt}^{1} - \left[\theta_{o(l)t} - \theta_{r(l)t}\right] \leq M(1 - z_{lt}^{1}), \forall l, t \tag{24}$$

$$X_l f_{lt}^{1} - \left[\theta_{o(l)t} - \theta_{r(l)t}\right] \geq -M(1 - z_{lt}^{1}), \forall l, t \tag{25}$$

$$-\theta^{max} \leq \theta_{nt} \leq \theta^{max}, \forall n, t \tag{26}$$

$$d_{it}^{k} - \delta_{ijt}^{k\to m}\hat{d}_{it}^{k} \geq 0, \forall (i,j) \in F_{i,j}^{k\to m} \cup M_{i,j}^{k\to m}, \forall t \tag{27}$$

$$g_{jt}^{m} - \delta_{ijt}^{k\to m}\bar{g}_{j}^{m} \leq 0, \forall (i,j) \in F_{i,j}^{k\to m}, \forall t \tag{28}$$

$$d_{jt}^{m} - \delta_{ijt}^{k\to m}\hat{d}_{jt}^{m} \leq 0, \forall (i,j) \in F_{i,j}^{k\to m}, \forall t \tag{29}$$

$$-\delta_{ijt}^{k\to m}\bar{f}_{l}^{m} \leq f_{lt}^{m} \leq \delta_{ijt}^{k\to m}\bar{f}_{l}^{m}, \forall (i,j) \in F_{i,j}^{k\to m}, l \in L_{j}^{m,nbr}, \forall t \tag{30}$$

$$-\delta_{ijt}^{k\to m}\bar{f}_{j}^{m} - (1 - \delta_{ijt}^{k\to m})\tilde{f}_{j}^{m} \leq f_{jt}^{m} \leq \delta_{ijt}^{k\to m}\bar{f}_{j}^{m} + (1 - \delta_{ijt}^{k\to m})\tilde{f}_{j}^{m}, \forall (i,j) \in M_{i,j}^{k\to m}, \forall t\Big\} \tag{31}$$

where (20)-(23) are the general flow constraints for the power and gas networks (and possibly other networks considered). Constraint (20) enforces the flow balance at each node for all the networks. Constraint (21) limits the capacities of generation units in each network. Constraint (22) bounds the maximum value of served demand at each node for all the networks. Constraint (23) sets the limits of network flow on each lines. Constraints (24)-(25) impose the physical restrictions on flows specifically for the power network ($k = 1$), where M is a sufficiently large positive constraint (i.e., $M \geq 2\theta^{max}$) and Constraint (26) bounds phase angles for power network nodes.

Different types of interdependencies exist among CI networks. Rinaldi, Peerenboom et al. (2001) defined four principal classes of interdependencies: physical, cyber, geographic, and logical. For IPGNs, typical connections include: i) *sink-source* connections where a gas city gate can fuel a gas turbine engine, which is an electric generator, ii) *sink-sink* connections where a city gate requires some energy from an electrical load to regulate its valves, and iii) *sink-transmit* connections where compressors consume electricity from an electrical load to increase the pressure on a gas pipeline, as sufficient line pressure is a feasibility requirement for the gas network. All these interdependencies can be modeled by defining a set of ordered components pairs (i, j) associated with node i in one CI network and component (node or line) j in another network, where the interdependency relation for (i, j) works if the flow demand of node i is fully satisfied (Gong, Mitchell et al. 2014, González, Dueñas-Osorio et al. 2016, Ouyang 2017). For the former two types of interdependencies in IPGNs, component j will be completely failed if the interdependency relation for (i, j)

does not work. The *sink-transmit* connections in IPGNs are modeled as capacity reduction, i.e., the capacity of line j is reduced if the interdependency relation for (i, j) does not work (Coffrin, Van Hentenryck et al. 2012). For this, we define a binary variable $\delta_{ijt}^{k\to m}$ to represent the interdependency from node i in network k to component (node or line) j in network m at time t: $\delta_{ijt}^{k\to m} = 1$ if the interdependency works normally and $\delta_{ijt}^{k\to m} = 0$ otherwise. For each ordered pair $(i, j) \in F_{i,j}^{k\to m} \cup M_{i,j}^{k\to m}$, the interdependency works normally, i.e., $\delta_{ijt}^{k\to m} = 1$, only if the demand level at node i in network k is fully satisfied at time t, i.e., $d_{it}^k = \hat{d}_{it}^k$, as described by Constraint (27). For each node j in the ordered pair $(i, j) \in F_{i,j}^{k\to m}$, the flow generation is bounded by zero or its generation capacity, as stated by Constraint (28), and its demand level is bounded by zero or the required demand, as stated by Constraint (29). Furthermore, if node j is not functioning, all its attached lines will not work and the flow on these lines should be zero, as described by Constraint (30). Finally, Constraint (31) models the *sink-transmit* interdependencies in IPGNs: the capacity of line j in network m decreases from its normal level $\bar{f}_j^m$ to a reduced level $\tilde{f}_j^m$ ($\tilde{f}_j^m < \bar{f}_j^m$) if the demand of its dependent node i in network k is not fully satisfied ($\delta_{ijt}^{k\to m} = 0$).

It is important to note that although the interdependency model (27)-(31) is proposed for IPGNs, it is general enough to account for all kinds of physical, geographical and logical interdependencies among different CIs via the approach of antecedence-consequence ordered pairs (Coffrin, Van Hentenryck et al. 2012, Gong, Mitchell et al. 2014). Note that the upper level decision variables x_n^k as well as the medium-level ones z_{lt}^k are included in Constraints (20)-(31) and, thus, they influence the lower-level problem, i.e., the maximization of system resilience by response operation.

4. Solution technique

In general, solving two-stage adaptive robust models is difficult because their multilevel optimization structure often gives rise to NP-hard problems (Ruiz and Conejo 2015). Several solution algorithms extended from the Benders' decomposition have been designed to address these problems. In these methods, the first stage objective function is gradually reconstructed using dual information from the second stage problem (Yao, Edmunds et al. 2007, Thiele, Terry et al. 2009, Bertsimas, Litvinov et al. 2013, Jabr 2013, Alguacil, Delgadillo et al. 2014). Regarding the proposed ARO model (9)-(31), however, the existence of the binary interdependency variables $\delta_{ij}^{k\to m}$ in the third level prevents the merging of the two inner problems, i.e. the second and third level min-max problems, into a single min problem using the Karush-Kuhn-Tucker (KKT) conditions (or the strong duality) of the third level max problem. Therefore, solution methods that depend

on the gradual reconstruction of the upper stage problem using dual information from the lower stage are inapplicable.

In this paper, we adopt a cutting plane strategy, which is based on primal cuts (Zeng and Zhao 2013), involving only primal decision variables, and we adapt its extended version, i.e., a nested column-and-row generation (NC&RG) method (Zhao and Zeng 2012), to solve the proposed two-stage ARO problem (9)-(31). Note that the uncertainty set defined by (12)-(17) is dependent on the first-stage decisions x_l^k, which makes the NC&RG not capable of being directly employed to solve the proposed ARO model (9)-(31) (Neyshabouri and Berg 2017). Next, in Section 4.1 we reformulate the ARO model (9)-(31) to its equivalent problem in which a new uncertainty set $\widetilde{\mathbb{U}}$ is defined so that it is independent on the first-stage decision variables and, then, in Section 4.2 we propose the main procedures for adapting the NC&RG algorithm to solve the reformulated ARO model.

4.1. Reformulation of uncertainty set

Observe that the uncertainty set $\mathbb{U}$ is dependent on the first-stage decision variables x_l^k only through Constraint (13), where x_l^k is a binary variable; thus, we have $\sum_{t\in\mathbb{T}} v_{lt}^k \leq 1 - x_l^k \leq 1\ \forall k, l$. Following this observation, we can relax Constraint (13) to

$$\sum_{t\in\mathbb{T}} v_{lt}^k \leq 1\ \forall k, l. \tag{32}$$

Then, the relaxed uncertainty set is defined by

$$\widetilde{\mathbb{U}} = \{\boldsymbol{u} | (6), (8)-(11), (26)\}. \tag{33}$$

To ensure the equivalence of the optimal solutions of the original ARO problem, a restricted feasible operation set $\widetilde{\mathbb{O}}(\boldsymbol{x}, \boldsymbol{u})$ should be defined. Actually, this can be achieved by substituting Constraints (23)-(25) in $\mathbb{O}(\boldsymbol{x}, \boldsymbol{u})$ with the following constraint:

$$-[x_l^k + z_{lt}^k(1 - x_l^k)]\bar{f}_l^k \leq f_{lt}^k \leq [x_l^k + z_{lt}^k(1 - x_l^k)]\bar{f}_l^k, \forall k, l, t. \tag{34}$$

$$X_l f_{lt}^1 - [\theta_{o(l)t} - \theta_{r(l)t}] \leq M\{1 - [x_l^1 + z_{lt}^1(1 - x_l^1)]\}, \forall l, t \tag{35}$$

$$X_l f_{lt}^1 - [\theta_{o(l)t} - \theta_{r(l)t}] \geq -M\{1 - [x_l^1 + z_{lt}^1(1 - x_l^1)]\}, \forall l, t \tag{36}$$

Then, the new restricted feasible operation set is given by

$$\widetilde{\mathbb{O}}(\boldsymbol{x},\boldsymbol{u}) = \{\boldsymbol{o} | (20)-(22),(26)-(31),(34)-(36)\}. \tag{37}$$

Consequently, we have the following middle-low level problem $\widetilde{\mathcal{H}}(\boldsymbol{x})$ based on the relaxed uncertainty set $\widetilde{\mathbb{U}}$ and restricted feasible operation set $\widetilde{\mathbb{O}}(\boldsymbol{x},\boldsymbol{u})$

$$\widetilde{\mathcal{H}}(\boldsymbol{x}) = \min_{\boldsymbol{u}\in\widetilde{\mathbb{U}}} \max_{\boldsymbol{o}\in\widetilde{\mathbb{O}}(\boldsymbol{x},\boldsymbol{u})} R(\boldsymbol{x},\boldsymbol{u},\boldsymbol{o}). \tag{38}$$

Observation 4.1. *For any given first stage decision vector* $\boldsymbol{x}$*,* $\widetilde{\mathcal{H}}(\boldsymbol{x})$ *is feasible since* $\boldsymbol{u} = [\boldsymbol{v},\boldsymbol{y},\boldsymbol{z}] = [\boldsymbol{0},\boldsymbol{0},\boldsymbol{1}]$ *and* $\boldsymbol{o} = [\boldsymbol{\theta},\boldsymbol{f},\boldsymbol{g},\boldsymbol{d},\boldsymbol{\delta}] = \boldsymbol{0}$ *is always a feasible solution.*

Proposition 4.1. *Given a fixed first stage decision vector* $\boldsymbol{x}$*, for any* $\widetilde{\boldsymbol{u}} \in \widetilde{\mathbb{U}}$*, there exists a* $\boldsymbol{u} \in \mathbb{U}(\boldsymbol{x})$ *so that* $\mathbb{O}(\boldsymbol{x},\boldsymbol{u}) = \widetilde{\mathbb{O}}(\boldsymbol{x},\widetilde{\boldsymbol{u}})$.

Proof. It suffices to find a vector $\boldsymbol{u} \in \mathbb{U}(\boldsymbol{x})$ so that Constraints (34)-(36) are equivalent to Constraints (23)-(25) for any given $\widetilde{\boldsymbol{u}} \in \widetilde{\mathbb{U}}$ and for the given $\boldsymbol{x}$. Note that vector $\boldsymbol{x}$ has only 1 and 0 elements, i.e., $x_l^k = 1$ or 0.

i) For $x_l^k = 0$, Constraint (13) is equivalent to the Constraint (32) and Constraints (34)-(36) are equivalent to Constraints (23)-(25). Thus, we simply set $[v_{lt}^k, y_{lt}^k, z_{lt}^k] = [\tilde{v}_{lt}^k, \tilde{y}_{lt}^k, \tilde{z}_{lt}^k]$ $\forall t \in \mathbb{T}$ for any feasible $[\tilde{v}_{lt}^k, \tilde{y}_{lt}^k, \tilde{z}_{lt}^k]$;

ii) For $x_l^k = 1$, the item $x_l^k + z_{lt}^k(1-x_l^k)$ in Constraint (34) and the item $x_l^1 + z_{lt}^1(1-x_l^1)$ in Constraints (35)-(36) for $\widetilde{\mathbb{O}}(\boldsymbol{x},\widetilde{\boldsymbol{u}})$ are both equal to 1 for all $t \in \mathbb{T}$. On the other side, for $\mathbb{U}(\boldsymbol{x})$, we have $\sum_{t\in\mathbb{T}} v_{lt}^k \le 1 - x_l^k = 1$, and $v_{lt}^k = 0$ for all $t \in \mathbb{T}$ because of the non-negativity of v_{lt}^k. Then, according to Constraint (16), we have $z_{lt}^k = 1$ for all $t \in \mathbb{T}$. Thus, Constraints (23)-(25) in $\mathbb{O}(\boldsymbol{x},\boldsymbol{u})$ are exactly the same with Constraints (34)-(36) in $\widetilde{\mathbb{O}}(\boldsymbol{x},\widetilde{\boldsymbol{u}})$ for $\forall t \in \mathbb{T}$. Consequently, we can set $[v_{lt}^k, y_{lt}^k, z_{lt}^k] = [0, \tilde{y}_{lt}^k, 1]$ for all $t \in \mathbb{T}$.

Therefore, the value of the vector $\boldsymbol{u} \in \mathbb{U}(\boldsymbol{x})$ has been found so that $\widetilde{\mathbb{O}}(\boldsymbol{x},\widetilde{\boldsymbol{u}}) = \mathbb{O}(\boldsymbol{x},\boldsymbol{u})$. ■

From Proposition 4.1, we can make the following statement:

Proposition 4.2. *Given any first stage decision vector* $\boldsymbol{x}$*, problem* $\widetilde{\mathcal{H}}(\boldsymbol{x})$ *is equivalent to the original middle-low level problem* $\mathcal{H}(\boldsymbol{x})$.

Proof. The proof is straightforward due the Proposition 4.1 and the fact that $\mathbb{U}(\boldsymbol{x}) \subseteq \widetilde{\mathbb{U}}$ for any $\boldsymbol{x}$. ■

Therefore, the original ARO model (9)-(31) is equivalent to the following first-stage decision-independent problem: $\max_{\boldsymbol{x}} \widetilde{\mathcal{H}}(\boldsymbol{x})$ subject to Constraints (10)(11), which can be rewritten in a compact form:

$$\max_{\boldsymbol{x}} \min_{\boldsymbol{u}\in\widetilde{\mathbb{U}}} \max_{\boldsymbol{h},\boldsymbol{\delta}\in\widetilde{\mathbb{O}}(\boldsymbol{x},\boldsymbol{u})} \boldsymbol{b}^T\boldsymbol{h} \tag{39}$$

s.t.

$$\boldsymbol{c}\boldsymbol{x} \leq B_P, \boldsymbol{x} \in \{0,1\}^{m_1} \tag{40}$$

$$\widetilde{\mathbb{U}} = \{\boldsymbol{u} \in \{0,1\}^{m_2} | \boldsymbol{P}\boldsymbol{u} \leq \boldsymbol{g}\} \tag{41}$$

$$\widetilde{\mathbb{O}}(\boldsymbol{x}, \widetilde{\boldsymbol{u}}) = \{\boldsymbol{h} \in \mathbb{R}^{m_3}, \boldsymbol{\delta} \in \{0,1\}^{m_4} | \boldsymbol{R}\boldsymbol{h} + \boldsymbol{W}\boldsymbol{\delta} \leq \boldsymbol{q} - \boldsymbol{H}\boldsymbol{x} - \boldsymbol{T}\boldsymbol{u}\} \tag{42}$$

where Constraint (40) corresponds to Constraints (10)(11), Constraint (41) corresponds to Constraint (33), Constraint (42) corresponds to Constraint (37), $\boldsymbol{x}$ is the binary first-stage decision vector, $\boldsymbol{u}$ is the uncertainty vector, $\boldsymbol{h}$ represents the continuous operation variables $\theta_{nt}, f_{lt}^k, g_{nt}^k, d_{nt}^k$ and $\boldsymbol{\delta}$ represents the binary interdependency variables. Matrices $\boldsymbol{P}, \boldsymbol{R}, \boldsymbol{W}, \boldsymbol{H}, \boldsymbol{T}$ contain the coefficients of variables in the constraints and vectors $\boldsymbol{g}, \boldsymbol{q}$ contain the right-hand side parameters in the constraints. m_1, m_2, m_3, m_4 are the dimensions of the vector spaces of variables $\boldsymbol{x}, \boldsymbol{u}, \boldsymbol{h}$ and $\boldsymbol{\delta}$ respectively, and vector $\boldsymbol{b}$ is the coefficient vector of variables in the objective function.

In the next subsection, we outline the steps of the exact procedure of the adapted NC&RG algorithm for the solution of the equivalent problem. For clarity, the compact formulation (39)-(42) is used.

4.2. Solution procedure

4.2.1. Inner C&RG for Middle Lower-Level Problem $\widetilde{\mathcal{H}}(x)$

With fixed first-stage decision $\boldsymbol{x}^*$, middle-level binary variable $\boldsymbol{u}^*$ and lower-level binary variable $\boldsymbol{\delta}^*$, the lower level maximization problem becomes

$$\max_{\boldsymbol{h}} \boldsymbol{b}^T\boldsymbol{h} \tag{43}$$

$$\text{s.t. } \boldsymbol{R}\boldsymbol{h} \leq \boldsymbol{q} - \boldsymbol{H}\boldsymbol{x}^* - \boldsymbol{T}\boldsymbol{u}^* - \boldsymbol{W}\boldsymbol{\delta}^*. \tag{44}$$

Then, this pure linear programming can be replaced by its dual form as follows

$$\min_{\boldsymbol{\lambda}}(\boldsymbol{q}-\boldsymbol{H}\boldsymbol{x}^*-\boldsymbol{T}\boldsymbol{u}^*-\boldsymbol{W}\boldsymbol{\delta}^*)^T\boldsymbol{\lambda} \tag{45}$$

$$\text{s.t. } \boldsymbol{R}^T\boldsymbol{\lambda}=\boldsymbol{b},\boldsymbol{\lambda}\geq\boldsymbol{0} \tag{46}$$

where $\boldsymbol{\lambda}$ is the dual variable. Then, the middle lower-level problem $\widetilde{\mathcal{H}}(\boldsymbol{x}^*)$ can be solved by the inner C&RG algorithm described below in Table 2.

Table 2. Inner C&RG algorithm for solving $\widetilde{\mathcal{H}}(\boldsymbol{x}^*)$

Step 1. Select an arbitrary feasible uncertainty scenario $\boldsymbol{u}^* \in \widetilde{\mathbb{U}}$, and solve the following inner subproblem:

$$\begin{aligned}&\max_{\boldsymbol{h},\boldsymbol{\delta}} \boldsymbol{b}^T\boldsymbol{h}\\ &\text{s.t. } \boldsymbol{R}\boldsymbol{h}+\boldsymbol{W}\boldsymbol{\delta}\leq\boldsymbol{q}-\boldsymbol{H}\boldsymbol{x}^*-\boldsymbol{T}\boldsymbol{u}^*.\end{aligned} \tag{47}$$

The obtained optimal solution is denoted by $(\boldsymbol{h}^*,\boldsymbol{\delta}^*)$; then, we set the upper bound $UB=\boldsymbol{b}^T\boldsymbol{h}^*$, the lower bound $LB=0$, the iteration counter $iter=1,\boldsymbol{\delta}^{1*}=\boldsymbol{\delta}^*$.

Step 2. Solve the following inner master problem:

$$\min_{\rho,\boldsymbol{u},\boldsymbol{\lambda}} \rho \tag{48}$$

$$\text{s.t. } \rho\geq(\boldsymbol{q}-\boldsymbol{H}\boldsymbol{x}^*-\boldsymbol{T}\boldsymbol{u}-\boldsymbol{W}\boldsymbol{\delta}^{i*})^T\boldsymbol{\lambda}^i, i=1,\dots iter \tag{49}$$

$$\boldsymbol{P}\boldsymbol{u}\leq\boldsymbol{g},\boldsymbol{u}\in\{0,1\}^{m_2} \tag{50}$$

$$\boldsymbol{R}^T\boldsymbol{\lambda}^i=\boldsymbol{b},\boldsymbol{\lambda}^i\geq\boldsymbol{0}, i=1,\dots iter. \tag{51}$$

Obtain the optimal objective value ρ^* and optimal solution $\boldsymbol{u}^*$. Update $LB=\rho^*$.

Step 3. Solve the inner subproblem (47) with $\boldsymbol{u}^*$ obtained in *Step 2*. Obtain the optimal solution $(\boldsymbol{h}^*,\boldsymbol{\delta}^*)$ and optimal objective value $\boldsymbol{b}^T\boldsymbol{h}^*$. Update the upper bound as $UB=\min\{UB,\boldsymbol{b}^T\boldsymbol{h}^*\}$.

Step 4. If $(UB-LB)/UB\leq\varepsilon_1$, terminate and return the optimal solution $(\boldsymbol{u}^*,\boldsymbol{h}^*,\boldsymbol{\delta}^*)$ and the optimal value $\widetilde{\mathcal{H}}^*(\boldsymbol{x}^*)=\rho^*$; otherwise, generate extra variables $\boldsymbol{\lambda}^{iter+1}$ and add related constraints (49) and (51) by setting $\boldsymbol{\delta}^{iter+1*}\leftarrow\boldsymbol{\delta}^*$ (where $\boldsymbol{\delta}^*$ is the optimal solution obtained from *Step 3*) to the inner master problem (48)-(51). Update $iter\leftarrow iter+1$ and continue with *Step 2*.

Note that there are bilinear terms involving $\boldsymbol{u}$ and $\boldsymbol{\lambda}^i$ in Constraint (49), which can be simply linearized due to the binary nature of $\boldsymbol{u}$. Therefore, the inner master problem and the inner subproblem are both

mixed integer linear programming (MILP) that can be solved efficiently by using standard branch-and-cut solvers.

4.2.2. Outer C&RG for Upper-Level Problem

Adopting a similar method to the inner C&RG algorithm, the outer C&RG algorithm for the upper-level problem identifies the optimal first-stage decision under all possible uncertainty scenarios, as described below in Table 3.

Table 3. Outer C&RG algorithm for upper-level problem

Step 1. Set $LB = 0, UB = +\infty$, and the iteration counter $iter = 1, \boldsymbol{u}^{1*} = [\boldsymbol{v}, \boldsymbol{y}, \boldsymbol{z}] = [\boldsymbol{0}, \boldsymbol{0}, \boldsymbol{1}]$.

Step 2. Solve the following outer master problem:

$$\max_{\varphi, \boldsymbol{x}, \boldsymbol{h}, \boldsymbol{\delta}} \varphi \tag{52}$$

$$\text{s.t. } \boldsymbol{cx} \le B_P, \boldsymbol{x} \in \{0,1\}^{m_1}. \tag{53}$$

$$\varphi \le \boldsymbol{b}^T \boldsymbol{h}^i, i = 1, \dots iter \tag{54}$$

$$\boldsymbol{Rh}^i + \boldsymbol{W\delta}^i + \boldsymbol{Hx} \le \boldsymbol{q} - \boldsymbol{Tu}^{i*}, \boldsymbol{h}^i \in \mathbb{R}^{m_3}, \boldsymbol{\delta}^i \in \{0,1\}^{m_4}, i = 1, \dots iter \tag{55}$$

Obtain the optimal solution $\boldsymbol{x}^*$ and the optimal value φ^*; update the upper bound as $UB = \min\{UB, \varphi^*\}$.

Step 3. Call the inner C&RG algorithm in Table 2 to solve the problem $\widetilde{\mathcal{H}}(\boldsymbol{x}^*)$ with $\boldsymbol{x}^*$ obtained in *Step 2;* obtain the optimal solution $(\boldsymbol{u}^*, \boldsymbol{h}^*, \boldsymbol{\delta}^*)$ and optimal value $\widetilde{\mathcal{H}}^*(\boldsymbol{x}^*)$, and update the lower bound as $LB = \max\left\{LB, \widetilde{\mathcal{H}}^*(\boldsymbol{x}^*)\right\}$.

Step 4. If $(UB - LB)/UB \le \varepsilon_2$, terminate and return the optimal solution $(\boldsymbol{x}^*, \boldsymbol{u}^*, \boldsymbol{h}^*, \boldsymbol{\delta}^*)$ and the optimal value φ^*; otherwise, generate extra variables $\boldsymbol{h}^{iter+1}, \boldsymbol{\delta}^{iter+1}$ and add related constraints (54)-(55) by setting $\boldsymbol{u}^{iter+1*} \leftarrow \boldsymbol{u}^*$ (where $\boldsymbol{u}^*$ is the optimal solution obtained from *Step 3*) to the outer master problem (52)-(55). Update $iter \leftarrow iter + 1$ and continue with *Step 2*.

Finally, the proposed two-stage ARO model (9)-(31) is reformulated to its equivalent problem (39)-(42), and, then, solved by adapting the nested C&RG algorithm. The convergence proof and the analysis of the convergence properties of this type of algorithms are provided in Zhao and Zeng (2012).

5. Case study

5.1. Dataset

This section presents numerical experiments of the proposed analysis framework on test IPGNs. The power system is the IEEE 24-bus one area reliability test system (Grigg, Wong et al. 1999), and the gas system is adapted from the IEEE 9-bus system (Ouyang and Fang 2017). To embed the systems into a specific territory, the line lengths and geographical locations are chosen following (Mohanpurkar, Sogbi et al. 2015). Bus P7 of the test power system is taken as a reference node and is located near Xiamen (24.5 N, 118.0E), a coastal city in China. The power and gas systems are georeferenced by projecting them onto a 400×400km^2 study area located in the South China, as illustrated in Figure 4. The detailed interdependencies between the two systems are given in Table 4 and are illustrated in Figure 3.

We assume for simplicity that only the conductor wires and support poles in the power system are vulnerable and can be damaged during the passage of a typhoon. The fragility curve data of power poles and lines are adopted from Panteli, Pickering et al. (2017). The hardening cost for an overhead line in the power system depends on the length of the line with a coefficient of \$1.0× 10^5 per km (Louth 2011), and a type of DG with 22MW unit capacity is considered to be placed in the system at an installation cost of \$1.0× 10^7 per unit.

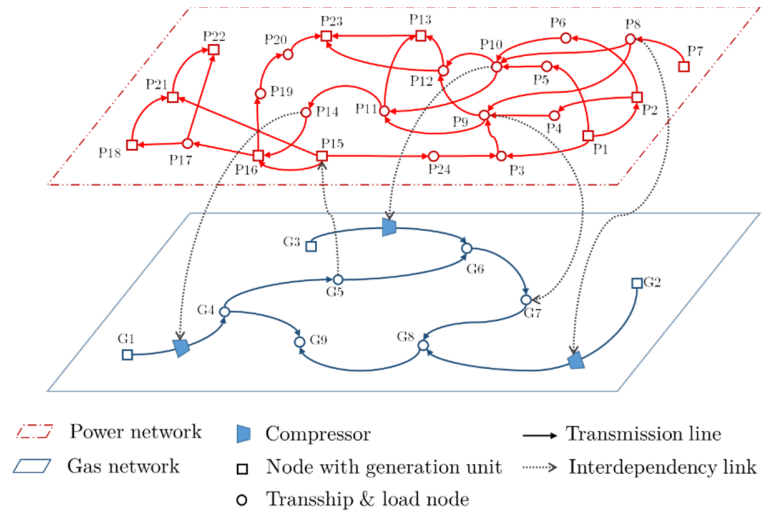

Figure 3. Interdependent power and gas systems.

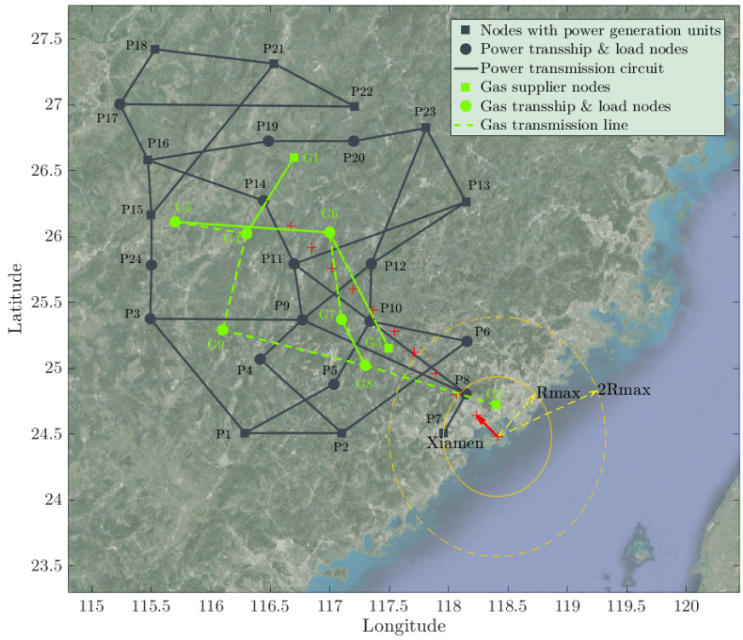

Figure 4. The georeferenced IPGNs and one realization of a typhoon track.

Table 4. The interdependencies between the power and gas systems

Ordered pairs (i, j)	Interdependency description
(P8,<G2,G8>)	*Sink-transmit* connection where the compressor on line <G2,G8> consumes electricity from electrical load node P8
(P9,G7)	*Sink-sink* connection where node G7 requires some energy from electrical load P9 to regulate its valves
(P10,<G3,G6>)	*Sink-transmit* connection where the compressor on line <G3,G6> consumes electricity from electrical load node P10
(P14,<G1,G4>)	*Sink-transmit* connection where the compressor on line <G1,G4> consumes electricity from electrical load node P14
(G5,P15)	*Sink-source* connection where the electric generators at node P15 consume gas from node G5 to generate electricity

5.2. Windstorm simulation

We consider four different scenarios of typhoon (a tropical windstorm that develops in the Northwestern Pacific Basin) with a category of "very strong" (sustained wind between 157–193 km/h) according to the RSMC Tokyo's Tropical Cyclone Intensity Scale. The tracks of the four typhoon scenarios are illustrated in Figure 5. Typhoons 1-3 share the same landfall location with latitude 24.50N and longitude 118.30E (near Xiamen). The typhoon track illustrated in Figure 4 corresponds to the typhoon scenario 1 in Figure 5. The red plus signs in Figure 4 represent the locations of the storm eye at different times, with one hour time steps. The inner yellow circles R_{max} in Figure 4 and Figure 5 indicate the boundary of the maximum winds for the traveling typhoons at their landfall points. The area between the yellow circle R_{max} and the dashed yellow circle $2R_{max}$ experiences around 82.5% of the maximum wind speed.

In order to assess the typhoon impact on the different elements of the system, its dynamic wind field is modeled through Equation (1), from which we can calculate the time-varying wind speeds at each location within the power system. Figure 6 shows the surface wind speed variations at bus P2 within the power system as the typhoons of the studied four scenarios travel along their tracks. One can find that bus P2 generally experiences the strongest wind threat during typhoon 3, since its track is the most geographically adjacent to P2.

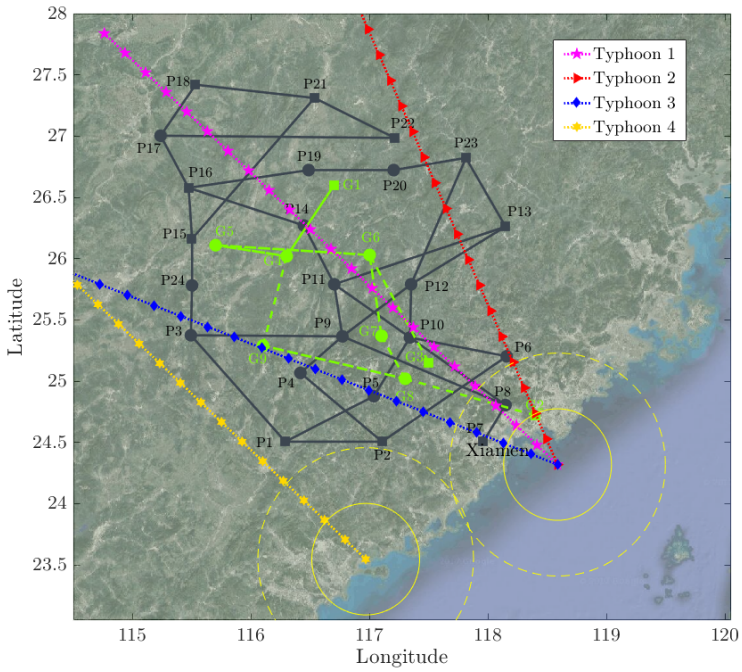

Figure 5. Tracks of 4 different typhoons with different landfall points and traveling directions.

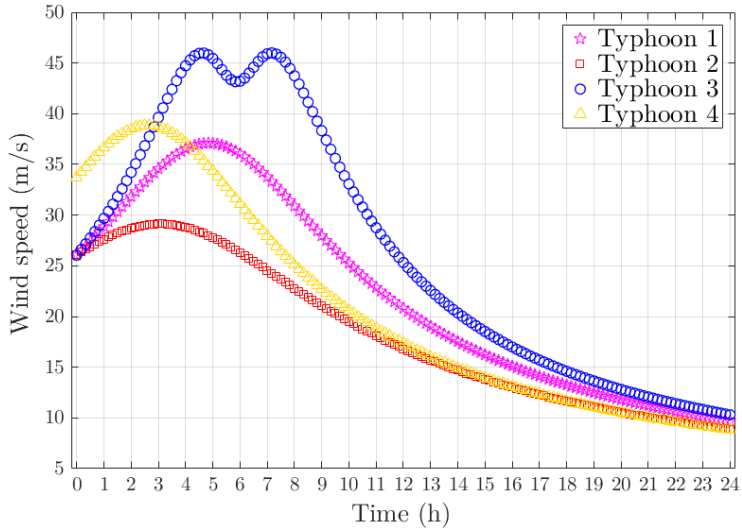

Figure 6. Hourly wind profiles at bus P2 under different scenarios of typhoons.

5.3. Results

Based on the above windstorm simulation and the geographic and structural fragility data of the test systems, the failure probability of transmission lines can be calculated using Equations (2)-(4). The recovery probabilities of failed lines are calculated by Equation (6), where the data for the MTTR and RS parameters of the transmission lines are based on Ouyang and Dueñas-Osorio (2014) and Espinoza, Panteli et al. (2016). The solution procedure proposed in Section 4.2 for the case study is implemented and solved in the IBM CPLEX 12.6 optimization studio. All calculations are performed on a laptop with 2.6-GHz CPU and 8GB RAM. The resilience weighting factor w^k is set as 0.5 for both the power and gas systems. The recovery uncertainty budget Υ is set as 0.1 for the power system. A tolerance level $\varepsilon_1 = \varepsilon_2 = 1.0 \times 10^{-5}$ is enforced for both the outer and inner layer C&RG algorithms.

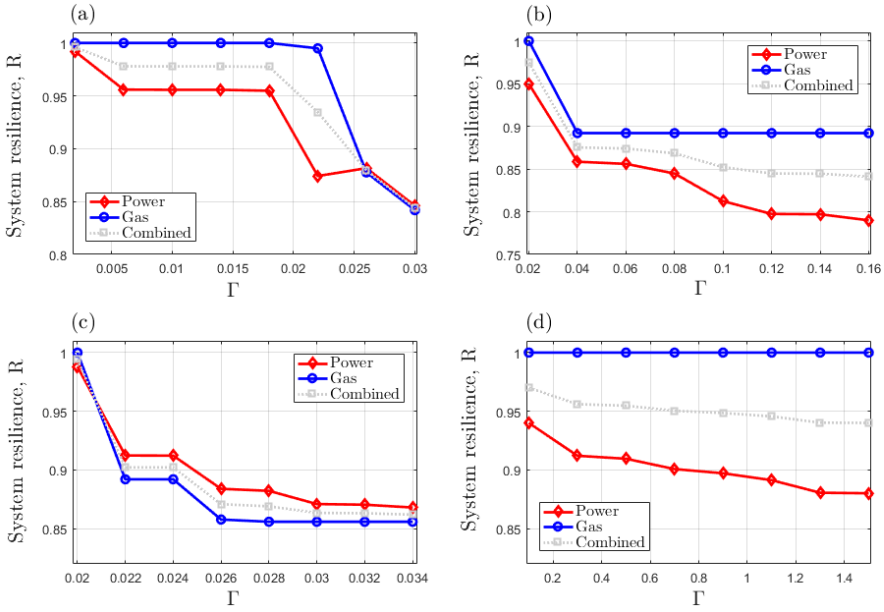

Figure 7. Optimal worst-case power and gas system resilience under different values of failure uncertainty budget Γ for typhoon (a) scenario 1, (b) scenario 2, (c) scenario 3, and (d) scenario 4, respectively, when there is no investment in resilience strategies, i.e., $B_P = \$0$.

We first investigate the case of no investment in resilience strategies (i.e. $B_P = \$0$). The proposed ARO model is solved for different values of failure uncertainty budget Γ for typhoon scenarios 1-4. Figure 7 presents the results of the optimized worst-case power and gas system resilience, i.e., R^{power} and R^{gas}, and their combination R for each scenarios. It can be seen that the combined power and gas system resilience decreases as the failure uncertainty budget Γ increases, for all the four typhoon scenarios. This is because a bigger value of Γ represents a larger upper limit of the number of failed lines, and the failure of a "reliable" line, i.e., having smaller failure probability p_{lt}^{power}, is increasingly allowed with an increased Γ. In other words, the decision maker allows more "surprising" events to happen by setting a larger value of Γ. For example, when $\Gamma = 0.002$ the optimal worst-case failed lines are 8-9, 11-13 and 17-22, resulting in a loss of the combined system resilience (i.e., $1 - R$) equal to 4.0×10^{-3} in typhoon scenario 1; when Γ is increased to 0.006 the worst-case failed lines are 2-6, 3-9, 8-9, 11-13, 12-23 and 17-22, resulting in a loss of the combined system resilience equal to 2.2×10^{-2}. Furthermore, Figure 7 shows that the resilience of the gas system is also deteriorated along with the decreased power system resilience for scenarios 1-3, due to the fact that the operations of some gas components (i.e., compressors and valves) are dependent on the incessant power supply from the corresponding electrical load buses. In scenario 4, the gas system is not affected since the

typhoon does not hit directly the power and gas systems, especially the interdependent components P8, P9, P10, and P14 (see Figure 5).

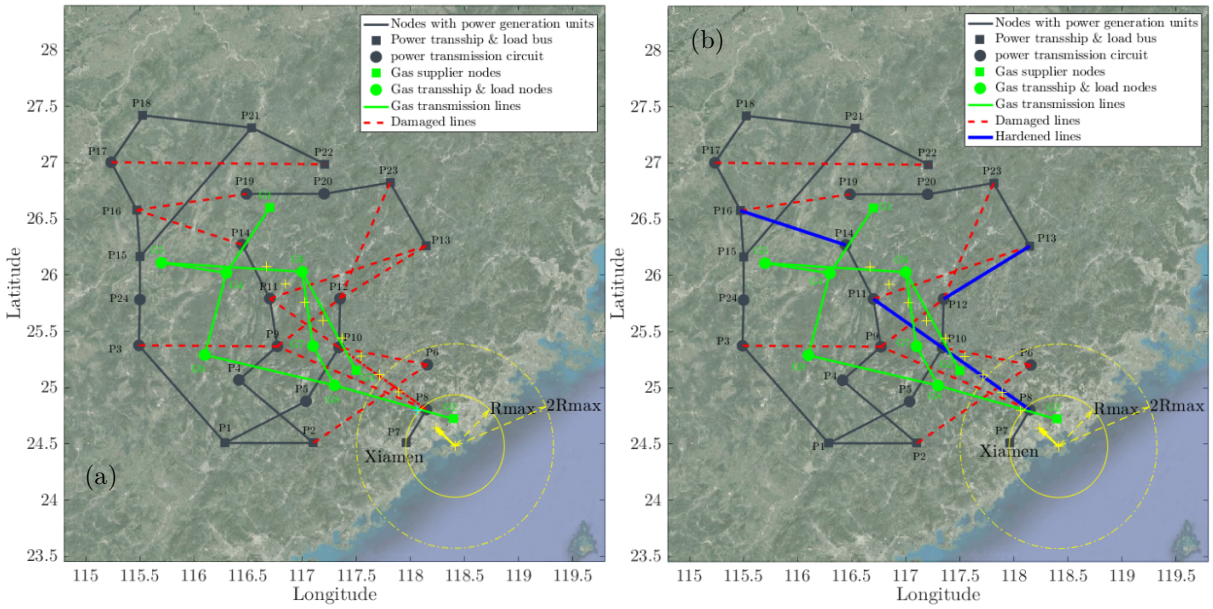

Figure 8. The power and gas systems (a) before and (b) after line hardening under typhoon scenario 1 and for $\Gamma = 0.026$ and investment budget $B_P = \$4.0 \times 10^7$.

Second, we consider hardening the power transmission lines (no DG unit placement) to protect against extreme winds induced by the typhoons. The hardening budget is assumed to be $B_P = \$4.0 \times 10^7$. By using the two-stage ARO model and solution algorithm proposed in Sections 3 and 4, the optimal hardening plan and worst-case system resilience can be calculated. Figure 8 shows the comparison of damaged lines before and after hardening under typhoon scenario 1 for $\Gamma = 0.026$. There are 13 damaged lines in the Figure 8(a) and damaged lines in Figure 8(b) has decreased to 9. Figure 8(b) also shows the locations and hardening strategies of transmission lines, where lines 8-10, 10-11, 12-13, and 14-16 are hardened. By this hardening strategy, the combined power and gas system resilience is enhanced from 0.880 to 0.970, which is an improvement of 10.23%.

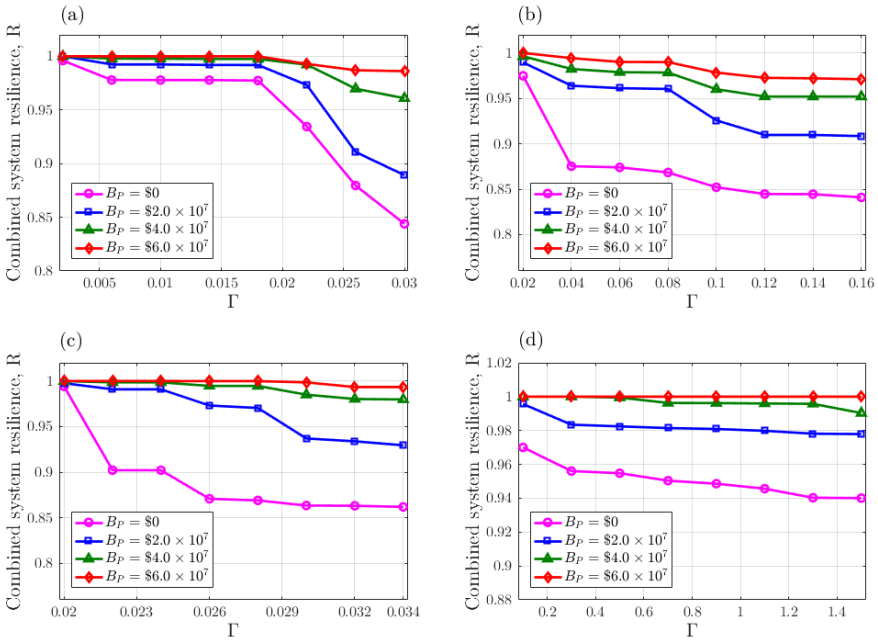

Figure 9. Optimal combined power and gas systems resilience along with Γ under different investment budgets $B_P = \$0, \$2.0 \times 10^7, \$4.0 \times 10^7$, and $\$6.0 \times 10^7$ for typhoon (a) scenario 1, (b) scenario 2, (c) scenario 3, and (d) scenario 4, respectively.

Figure 9 shows the combined system resilience along with Γ for different investment budgets and for the four typhoon scenarios studied. One can see that in the absence of protection, the post-hazard combined system resilience decreases the most rapidly with the value of failure uncertainty budget Γ. With each additional investment in protection, this curve becomes less steep, indicating improved operational resilience for the IPGNs. This is simply because additional transmission lines can be hardened when the investment budget is increased. Table 5 reports the detailed hardening plans under different investment budgets for the four typhoon scenarios (Γ is fixed for each scenario). Indeed, additional transmission lines are chosen to be hardened with each added investment budget, in most of the cases. However, it is noticed that the number of hardened lines is not increased when the investment budget is increased from $\$4.0 \times 10^7$ to $\$6.0 \times 10^7$ in scenario 4, but the hardened lines are changed, i.e., lines 2-4 and 15-16 are substituted by lines 2-6 and 3-9, which also leads to an enhancement of the combined system resilience from 0.990 to 1.000. This indicates that the optimal set of lines to be hardened in small budget situations is not necessarily a subset of the lines to be hardened in large budget situations. Therefore, the decision maker should evaluate carefully the available investment budget in order to obtain the optimal hardening plan.

Table 5. Optimal hardening plans for different typhoon scenarios and investment budgets

Typhoon scenario	Investment budget $B_P(\times 10^7\$)$	Set of transmission lines to be hardened	Combined resilience
1 ($\Gamma = 0.026$)	2.0	8-10, 12-13	0.911
	4.0	8-10, 10-11, 12-13, 14-16	0.970
	6.0	6-10, 9-12, 8-10, 10-11, 11-13, 12-13,	0.987
2 ($\Gamma = 0.1$)	2.0	8-10, 10-12	0.926
	4.0	8-10, 10-12, 12-13, 13-23, 20-23	0.960
	6.0	6-10, 8-9, 9-12, 10-12, 12-13, 12-23	0.978
3 ($\Gamma = 0.026$)	2.0	2-4, 8-10	0.973
	4.0	1-5, 2-6, 8-10, 9-12	0.995
	6.0	1-5, 2-4, 3-9, 8-9, 9-12	0.999
4 ($\Gamma = 1.5$)	2.0	3-24, 15-24	0.978
	4.0	1-5, 2-4, 3-24, 4-9, 15-16, 15-24	0.990
	6.0	1-5, 2-6, 3-9, 3-24, 4-9, 15-24	1.000

Third, to investigate the importance of DG in the IPGNs under NHs, a comparison among resilience strategies "without DG" and "with DG" is studied. In the case of "without DG", only transmission line hardening is allowed; in the case of "with DG", both the strategies of line hardening and DG unit allocation are allowed. Figure 10 shows the results of the combined power and gas system resilience as a function of the investment budget B_P for the two cases and for each of the studied scenarios. As can be seen from the Figure, the effectiveness of hardening in terms of enhanced interdependent system resilience is improved by DG allocation as the combined system resilience of "with DG" is generally larger than that of "without DG", except for typhoon scenario 4 where the two cases result in identical solutions. In fact, DG units are effective as a backup when a power system is damaged by a natural disaster: the loads in branches that are disconnected from the main grid can be picked up by a DG unit if available, forming so-called microgrids where the power can be supplied by the DG within the microgrid (Yuan, Wang et al. 2016). This result highlights the importance of coordinating the placement of DG units with transmission line hardening, or more generally coordinating different resilience strategies, in the pre-disruption investment planning for system resilience enhancement.

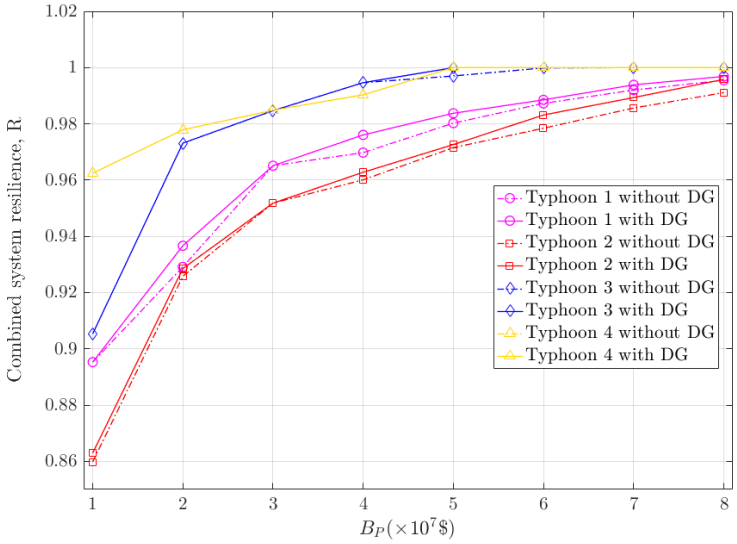

Figure 10. Impact of DG on combined system resilience. The failure uncertainty budget is fixed at $\Gamma = 0.026, 0.1, 0.026$ and 1.5 for typhoon scenarios 1, 2, 3, and 4, respectively.

In reality, a coordinated defense agency for different CIs may not exist. Thus, each system makes its own protection decisions without considering the interdependencies with other CIs. To investigate this case, we assume that the decision makers in the power system make the protection planning only for their own interest without considering the interdependencies with the gas network, i.e. the objective function in the proposed ARO model is the resilience of only the power system. We call this strategy "egotistic protection" to differentiate it from "coordinated protection" where the interdependent systems are protected as a whole. The protection solutions attained from the "egotistic" ARO model are tested under the worst case NH realization (i.e., a NH attacks the power system to minimize the combined power and gas resilience by taking into account their interdependencies) to obtain the power system resilience, gas system resilience and their combination. Figure 11 shows the comparison of the system resilience between the case of coordinated protection and the case of egotistic protection for typhoon scenarios 1-3 (in typhoon scenario 4 where the interdependencies are not affected, the two protection strategies obviously lead to the same results). It can be seen from the Figure that when the investment budget is small, the egotistic protection (diamond dash-dot lines) is able to increase marginally the power system resilience compared with the coordinated protection (diamond lines), nevertheless, this is achieved by compromising the resilience of the gas system considerably. That is, the gas system resilience in egotistic protection (circle dash-dot lines) decreases largely compared with that in coordinated protection (circle lines). The combined power and gas resilience in the case of egotistic protection (square dash-dot lines) is always smaller than or at most equal to that in the case of

coordinated protection (square lines). When the investment budget is increased, the two protection strategies gradually result in equivalent effects, since the power buses that support the operation of the gas system also come into the list of protection in the egotistic strategy. These results highlight the significance of protecting interdependent CIs as a whole against NHs, especially when the investment budget is relatively small.

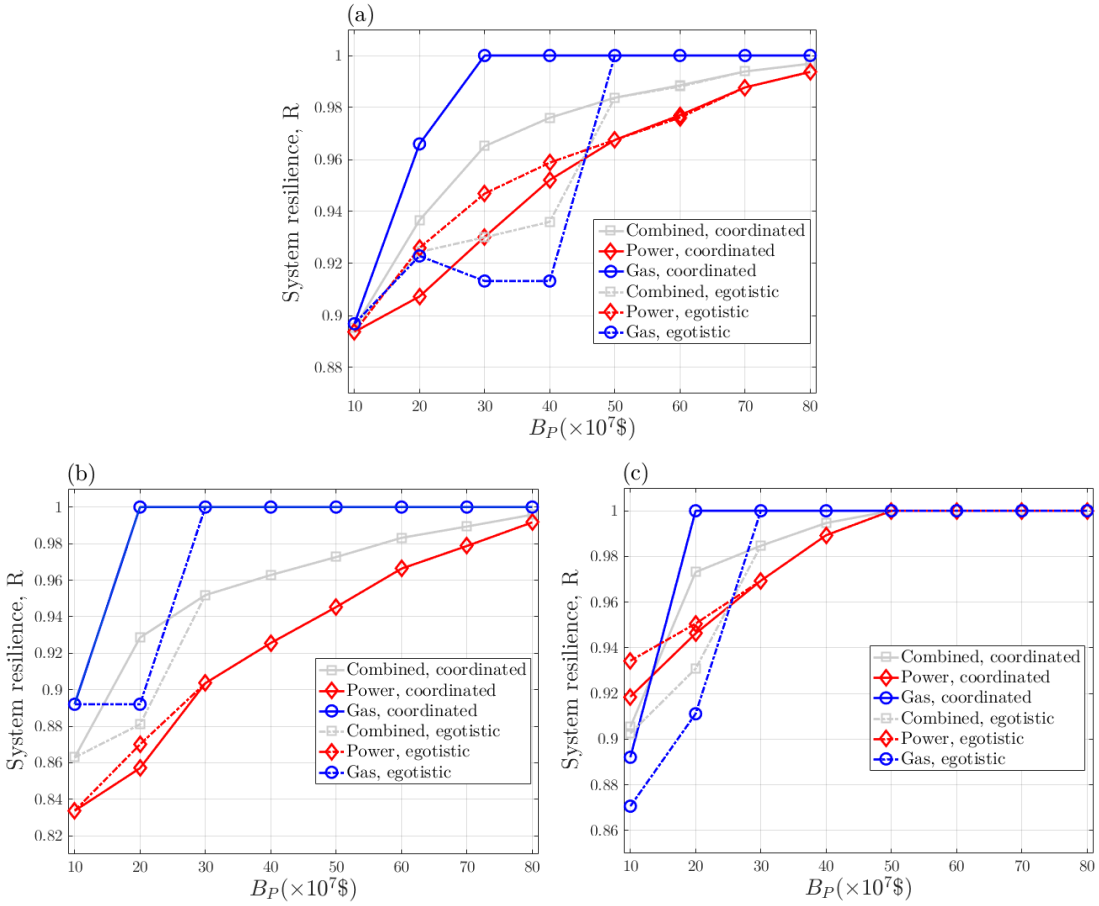

Figure 11. Comparison of power system, gas system and their combined resilience between the case of coordinated protection and the case of egotistic protection for typhoon scenarios (a) 1, (b) 2, and (c) 3, respectively; both transmission line hardening and DG placement are considered. The failure uncertainty budget is fixed at $\Gamma = 0.026, 0.1$, and 0.026 for scenarios 1, 2, and 3, respectively.

Finally, Figure 12 shows the computation times of the NC&RG algorithm for solving the proposed ARO model. It can be observed that the computation burden is relatively light for small values of failure uncertainty budget Γ and small investment budget B_P for each typhoon scenario. This is because the feasible hardening plans for small B_P and the number of transmission lines allowed to be failed for small Γ

are both limited. As the values of Γ and B_P are increased, the computational time largely increases, particularly for large values of failure uncertainty budget Γ. In fact, the investment budget B_P largely affect the feasibility region (solution space) of the outer-layer master problem (52), and the failure uncertainty budget Γ conditions the feasibility region (solution space) of the inner-layer master problem (48). The two MIP problems (48) and (52) are the most computationally demanding steps of the proposed method. In practice, the computational burden can be released by sophisticated MIP gap setting, e.g., the dynamic gap strategy for NC&RG (Fang and Sansavini 2017), or allowance of a larger converging tolerance level ε_1 and ε_2.

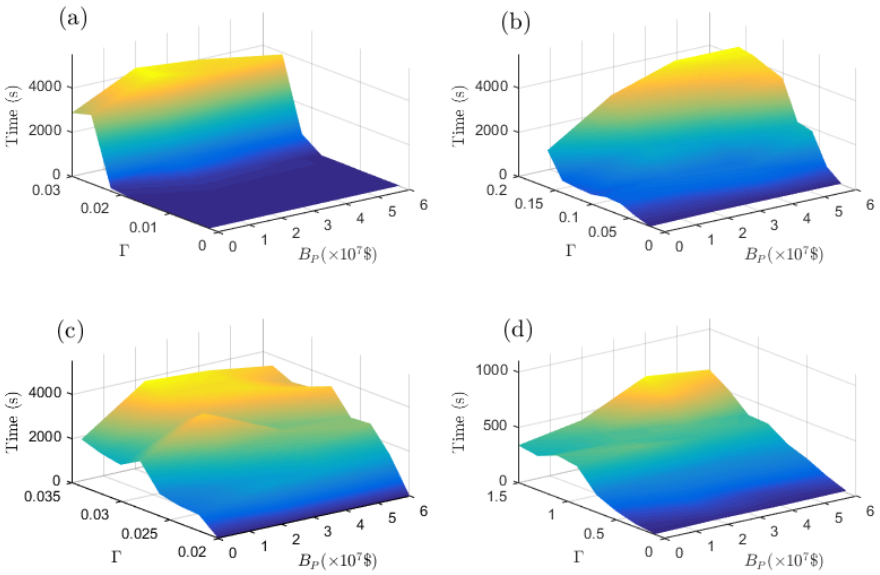

Figure 12. Computational performance of the optimization algorithm for typhoon (a) scenario 1, (b) scenario 2, (c) scenario 3, and (d) scenario 4, respectively.

6. Conclusions

This paper presents a novel ARO-based mathematical framework for enhancing the resilience of interdependent CIs against NHs. In this framework, the potential impacts of a specific NH on an infrastructure are firstly evaluated, in terms of failure and recovery probabilities of system components; these are, then, fed into a two-stage ARO model to determine the optimal planning of resilience strategies under limited investment budget, anticipating the worst possible realization of the uncertainty of component failures under the NH. More specifically, in the first stage, the optimal investment planning under a limited budget is sought by maximizing the resilience of the interdependent CIs, which is done by anticipating that,

right after this decision is made, the NH will behave in the worst possible manner given the forecasted but uncertain information of the NH. In the second stage, right after the worst uncertainty outcome is realized, the interdependent CIs will try to adapt to it via response operations, in order to minimize the impact caused by the NH. This approach bridges the gap between the difficulties of accurately predicting the hazard information in the classical probability-based analyses and the over-conservatism of the pure worst-case-oriented models for CI resilience under a specific NH, thus, providing a useful tool to help decision-makers in making more-informed pre-hazard preparation decisions.

Mathematically, the proposed model configures a tri-level max-min-max MIP with discrete variables existed in the innermost layer, which is challenging to be solved directly. For its solution, we adopt a cutting plane strategy which is based on primal cuts, involving only primal decision variables, and we adapt its extended version, called the NC&RG method to solve the proposed two-stage ARO problem. The application to a case study concerning the resilience of IPGNs under simulated wind storms demonstrates the effectiveness of the proposed model and solution method.

Some managerial insights can be drawn from the specific case study including: 1) investment in pre-hazard resilience strategies, e.g., transmission line hardening and DG placement, can effectively improve the resilience of IPGNs against typhoons; however, the optimal set of lines to be hardened is sensitive to the amount of investment budget. Thus, the decision maker should evaluate carefully the available budget in order to obtain the optimal plan for implementation. 2) Considering the combination of different resilience strategies can be more effective for system resilience enhancement. 3) When the investment budget is relatively small, it is significant to protect different CIs as a whole and consider their interdependency in order to achieve a globally optimum resilience enhancement plan against NHs.

Reference

Adachi, T. and B. R. Ellingwood (2008). "Serviceability of earthquake-damaged water systems: Effects of electrical power availability and power backup systems on system vulnerability." Reliability engineering & system safety **93**(1): 78-88.

Aerts, J. C., N. Lin, W. Botzen, K. Emanuel and H. de Moel (2013). "Low-Probability Flood Risk Modeling for New York City." Risk Analysis **33**(5): 772-788.

Alderson, D. L., G. G. Brown and W. M. Carlyle (2015). "Operational models of infrastructure resilience." Risk Analysis **35**(4): 562-586.

Alderson, D. L., G. G. Brown, W. M. Carlyle and R. K. Wood (NAVAL POSTGRADUATE SCHOOL MONTEREY CA DEPT OF OPERATIONS RESEARCH) (2011). "Solving defender-attacker-defender models for infrastructure defense." Available at: Accessed

Alguacil, N., A. Delgadillo and J. M. Arroyo (2014). "A trilevel programming approach for electric grid defense planning." Computers & Operations Research **41**: 282-290.

Australian Government (2010). "Critical infrastructure resilience strategy." Available at: https://www.tisn.gov.au/Documents/Australian+Government+s+Critical+Infrastructure+Resilience+Strategy.pdf, Accessed October 12, 2017.

Batke, S. P., M. Jocque and D. L. Kelly (2014). "Modelling hurricane exposure and wind speed on a mesoclimate scale: a case study from Cusuco NP, Honduras." PloS one **9**(3): e91306.

Bayliss, C., C. R. Bayliss and B. J. Hardy (2012). Transmission and distribution electrical engineering, Elsevier.

Bertsimas, D., D. B. Brown and C. Caramanis (2011). "Theory and applications of robust optimization." SIAM review **53**(3): 464-501.

Bertsimas, D., E. Litvinov, X. A. Sun, J. Zhao and T. Zheng (2013). "Adaptive robust optimization for the security constrained unit commitment problem." IEEE Transactions on Power Systems **28**(1): 52-63.

Bhuiyan, M. and R. Allan (1994). "Inclusion of weather effects in composite system reliability evaluation using sequential simulation." IEE Proceedings-Generation, Transmission and Distribution **141**(6): 575-584.

Bjarnadottir, S., Y. Li and M. G. Stewart (2012). "Hurricane risk assessment of power distribution poles considering impacts of a changing climate." Journal of Infrastructure Systems **19**(1): 12-24.

Brown, G., M. Carlyle, J. Salmerón and K. Wood (2006). "Defending critical infrastructure." Interfaces **36**(6): 530-544.

Brown, R. (2009). "Cost-benefit analysis of the deployment of utility infrastructure upgrades and storm hardening programs." Quanta Technology, Raleigh.

Bruneau, M., S. E. Chang, R. T. Eguchi, G. C. Lee, T. D. O'Rourke, A. M. Reinhorn, M. Shinozuka, K. Tierney, W. A. Wallace and D. Von Winterfeldt (2003). "A framework to quantitatively assess and enhance the seismic resilience of communities." Earthquake spectra **19**(4): 733-752.

Buldyrev, S. V., R. Parshani, G. Paul, H. E. Stanley and S. Havlin (2009). "Catastrophic cascade of failures in interdependent networks." arXiv preprint arXiv:0907.1182.

Campbell, R. J. (2012). Weather-related power outages and electric system resiliency, Congressional Research Service, Library of Congress Washington, DC.

Canham, C. D., M. J. Papaik and E. F. Latty (2001). "Interspecific variation in susceptibility to windthrow as a function of tree size and storm severity for northern temperate tree species." Canadian Journal of Forest Research **31**(1): 1-10.

Coffrin, C., P. Van Hentenryck and R. Bent (2012). Last-Mile Restoration for Multiple Interdependent Infrastructures. AAAI.

Commission of the European Communities (2006). "Communication from the Commission on a European Programme for Critical Infrastructure Protection." Available at: http://eur-lex.europa.eu/LexUriServ/LexUriServ.do?uri=COM:2006:0786:FIN:EN:PDF, Accessed October 12, 2017.

Cutter, S. L., A. Ismail-Zadeh, I. Alcantara-Ayala, O. Altan, D. N. Baker, S. Briceno, H. Gupta, A. Holloway, D. Johnston and G. A. McBean (2015). "Global risks: pool knowledge to stem losses from disasters." Nature **522**(7556).

Davis, C., W. Wang, S. S. Chen, Y. Chen, K. Corbosiero, M. DeMaria, J. Dudhia, G. Holland, J. Klemp and J. Michalakes (2008). "Prediction of landfalling hurricanes with the advanced hurricane WRF model." Monthly Weather Review **136**(6): 1990-2005.

Department for Environment (Food & Rural Affairs) (2011). "Climate resilient infrastructure: preparing for a changing climate." Available at: https://www.gov.uk/government/publications/climate-resilient-infrastructure-preparing-for-a-changing-climate--2, Accessed October 12, 2017.

Duffey, R. B. and T. Ha (2013). "The probability and timing of power system restoration." IEEE Transactions on power Systems **28**(1): 3-9.

Espinoza, S., M. Panteli, P. Mancarella and H. Rudnick (2016). "Multi-phase assessment and adaptation of power systems resilience to natural hazards." Electric Power Systems Research **136**: 352-361.

Fang, Y.-P., N. Pedroni and E. Zio (2016). "Resilience-based component importance measures for critical infrastructure network systems." IEEE Transactions on Reliability **65**(2): 502-512.

Fang, Y., N. Pedroni and E. Zio (2015). "Optimization of Cascade-Resilient Electrical Infrastructures and its Validation by Power Flow Modeling." Risk Analysis **35**(4): 594-607.

Fang, Y. and G. Sansavini (2017). "Emergence of Antifragility by Optimum Postdisruption Restoration Planning of Infrastructure Networks." Journal of Infrastructure Systems **23**(4): 04017024.

Fang, Y. and G. Sansavini (2017). "Optimizing power system investments and resilience against attacks." Reliability Engineering & System Safety **159**: 161-173.

Fang, Y., G. Sansavini and Z. Enrico (2017). "An Optimization-Based Mathematical Framework for the Identification of Infrastructure Vulnerabilities under Natural Hazards." Risk Analysis **Under review**.

Franchin, P. and F. Cavalieri (2015). "Probabilistic assessment of civil infrastructure resilience to earthquakes." Computer-Aided Civil and Infrastructure Engineering **30**(7): 583-600.

Gong, J., J. E. Mitchell, A. Krishnamurthy and W. A. Wallace (2014). "An interdependent layered network model for a resilient supply chain." Omega **46**: 104-116.

González, A. D., L. Dueñas-Osorio, M. Sánchez-Silva and A. L. Medaglia (2016). "The interdependent network design problem for optimal infrastructure system restoration." Computer-Aided Civil and Infrastructure Engineering **31**(5): 334-350.

Grigg, C., P. Wong, P. Albrecht, R. Allan, M. Bhavaraju, R. Billinton, Q. Chen, C. Fong, S. Haddad and S. Kuruganty (1999). "The IEEE reliability test system-1996. A report prepared by the reliability test system task force of the application of probability methods subcommittee." IEEE Transactions on power systems **14**(3): 1010-1020.

Han, S. R., S. D. Guikema and S. M. Quiring (2009). "Improving the predictive accuracy of hurricane power outage forecasts using generalized additive models." Risk analysis **29**(10): 1443-1453.

Hangan, H., E. Savory, A. El Damatty, J. Galsworthy and C. Miller (2008). Modeling and prediction of failure of transmission lines due to high intensity winds. Structures Congress 2008: Crossing Borders.

He, F. and J. Zhuang (2016). "Balancing pre-disaster preparedness and post-disaster relief." European Journal of Operational Research **252**(1): 246-256.

Holland, G. J., J. I. Belanger and A. Fritz (2010). "A revised model for radial profiles of hurricane winds." Monthly Weather Review **138**(12): 4393-4401.

Hosseini, S., K. Barker and J. E. Ramirez-Marquez (2016). "A review of definitions and measures of system resilience." Reliability Engineering & System Safety **145**: 47-61.

Jabr, R. (2013). "Robust transmission network expansion planning with uncertain renewable generation and loads." IEEE Transactions on Power Systems **28**(4): 4558-4567.

Kröger, W. and E. Zio (2011). Vulnerable systems, Springer Science & Business Media.

Lee II, E. E., J. E. Mitchell and W. A. Wallace (2007). "Restoration of services in interdependent infrastructure systems: A network flows approach." IEEE Transactions on Systems, Man, and Cybernetics, Part C (Applications and Reviews) **37**(6): 1303-1317.

Li, G., P. Zhang, P. B. Luh, W. Li, Z. Bie, C. Serna and Z. Zhao (2014). "Risk analysis for distribution systems in the northeast US under wind storms." IEEE Transactions on Power Systems **29**(2): 889-898.

Li, Y. and B. R. Ellingwood (2006). "Hurricane damage to residential construction in the US: Importance of uncertainty modeling in risk assessment." Engineering structures **28**(7): 1009-1018.

Lin, N., K. Emanuel, M. Oppenheimer and E. Vanmarcke (2012). "Physically based assessment of hurricane surge threat under climate change." Nature Climate Change **2**(6): 462.

Lindell, M. K. and C. S. Prater (2003). "Assessing community impacts of natural disasters." Natural hazards review **4**(4): 176-185.

Liu, H., R. A. Davidson and T. V. Apanasovich (2007). "Statistical forecasting of electric power restoration times in hurricanes and ice storms." IEEE Transactions on Power Systems **22**(4): 2270-2279.

Losada, C., M. P. Scaparra and J. R. O'Hanley (2012). "Optimizing system resilience: a facility protection model with recovery time." European Journal of Operational Research **217**(3): 519-530.

Louth, D. (Connecticut Light & Power) (2011). "Governor's Two-Storm Panel: Distribution Infrastructure Hardening Options and Recommendations." Available at: http://www.ctconstruction.org/files/public/Two_Storm_Panel_Storm_Hardening.pdf, Accessed October 2017.

MacKenzie, C. A. and C. W. Zobel (2016). "Allocating Resources to Enhance Resilience, with Application to Superstorm Sandy and an Electric Utility." Risk Analysis **36**(4): 847-862.

Mohanpurkar, M., H. V. Sogbi and S. Suryanarayanan (2015). Geographical Information Systems and Loop Flows in Power Systems. Electric Power Engineering Research and Education, Springer**:** 135-153.

Montz, B. E., G. A. Tobin and R. R. Hagelman III (2017). Natural hazards: explanation and integration, Guilford Publications.

Nateghi, R., S. D. Guikema and S. M. Quiring (2011). "Comparison and validation of statistical methods for predicting power outage durations in the event of hurricanes." Risk analysis **31**(12): 1897-1906.

Neyshabouri, S. and B. P. Berg (2017). "Two-stage robust optimization approach to elective surgery and downstream capacity planning." European Journal of Operational Research **260**(1): 21-40.

NOAA (2016). "Tracking data of the Typhoon Meranti."

Nurre, S. G., B. Cavdaroglu, J. E. Mitchell, T. C. Sharkey and W. A. Wallace (2012). "Restoring infrastructure systems: An integrated network design and scheduling (INDS) problem." European Journal of Operational Research **223**(3): 794-806.

Ouyang, M. (2014). "Review on modeling and simulation of interdependent critical infrastructure systems." Reliability engineering & System safety **121**: 43-60.

Ouyang, M. (2017). "A mathematical framework to optimize resilience of interdependent critical infrastructure systems under spatially localized attacks." European Journal of Operational Research **262**(3): 1072-1084.

Ouyang, M. and L. Dueñas-Osorio (2014). "Multi-dimensional hurricane resilience assessment of electric power systems." Structural Safety **48**: 15-24.

Ouyang, M. and Y. Fang (2017). "A mathematical framework to optimize critical infrastructure resilience against intentional attacks." Computer-Aided Civil and Infrastructure Engineering.

Panteli, M. and P. Mancarella (2015). "Influence of extreme weather and climate change on the resilience of power systems: Impacts and possible mitigation strategies." Electric Power Systems Research **127**: 259-270.

Panteli, M. and P. Mancarella (2015). "Modeling and evaluating the resilience of critical electrical power infrastructure to extreme weather events." IEEE Systems Journal.

Panteli, M., C. Pickering, S. Wilkinson, R. Dawson and P. Mancarella (2017). "Power System Resilience to Extreme Weather: Fragility Modeling, Probabilistic Impact Assessment, and Adaptation Measures." IEEE Transactions on Power Systems **32**(5): 3747-3757.

Pidgeon, N. (2012). "Climate change risk perception and communication: addressing a critical moment?" Risk Analysis **32**(6): 951-956.

Presidential Policy Directive (PPP) (2013). "Critical Infrastructure Security and Resilience." PPD-21, Available at: https://obamawhitehouse.archives.gov/the-press-office/2013/02/12/presidential-policy-directive-critical-infrastructure-security-and-resil, Accessed October 12, 2017.

Rinaldi, S. M., J. P. Peerenboom and T. K. Kelly (2001). "Identifying, understanding, and analyzing critical infrastructure interdependencies." IEEE Control Systems **21**(6): 11-25.

Rocchetta, R., Y. Li and E. Zio (2015). "Risk assessment and risk-cost optimization of distributed power generation systems considering extreme weather conditions." Reliability Engineering & System Safety **136**: 47-61.

Ruiz, C. and A. J. Conejo (2015). "Robust transmission expansion planning." European Journal of Operational Research **242**(2): 390-401.

Salman, A. M., Y. Li and M. G. Stewart (2015). "Evaluating system reliability and targeted hardening strategies of power distribution systems subjected to hurricanes." Reliability Engineering & System Safety **144**: 319-333.

Savory, E., G. A. Parke, M. Zeinoddini, N. Toy and P. Disney (2001). "Modelling of tornado and microburst-induced wind loading and failure of a lattice transmission tower." Engineering structures **23**(4): 365-375.

Scaparra, M. P. and R. L. Church (2008). "A bilevel mixed-integer program for critical infrastructure protection planning." Computers & Operations Research **35**(6): 1905-1923.

Shannon, C. E. and W. Weaver (1998). The mathematical theory of communication, University of Illinois press.

Sharkey, T. C., B. Cavdaroglu, H. Nguyen, J. Holman, J. E. Mitchell and W. A. Wallace (2015). "Interdependent network restoration: On the value of information-sharing." European Journal of Operational Research **244**(1): 309-321.

Thiele, A., T. Terry and M. Epelman (2009). "Robust linear optimization with recourse." Rapport technique: 4-37.

Vespignani, A. (2010). "Complex networks: The fragility of interdependency." Nature **464**(7291): 984-985.

Vickery, P. J. and P. F. Skerlj (2005). "Hurricane gust factors revisited." Journal of Structural Engineering **131**(5): 825-832.

Wang, Y., C. Chen, J. Wang and R. Baldick (2016). "Research on resilience of power systems under natural disasters—A review." IEEE Transactions on Power Systems **31**(2): 1604-1613.

Xie, Q. and R. Zhu (2011). "Earth, wind, and ice." IEEE Power and Energy Magazine **9**(2): 28-36.

Yao, Y., T. Edmunds, D. Papageorgiou and R. Alvarez (2007). "Trilevel optimization in power network defense." IEEE Transactions on Systems, Man, and Cybernetics, Part C (Applications and Reviews) **37**(4): 712-718.

Yuan, W., J. Wang, F. Qiu, C. Chen, C. Kang and B. Zeng (2016). "Robust optimization-based resilient distribution network planning against natural disasters." IEEE Transactions on Smart Grid **7**(6): 2817-2826.

Zapata, C., S. Silva, H. Gonzalez, O. Burbano and J. Hernandez (2008). Modeling the repair process of a power distribution system. Transmission and Distribution Conference and Exposition: Latin America, 2008 IEEE/PES, IEEE.

Zeng, B. and L. Zhao (2013). "Solving two-stage robust optimization problems using a column-and-constraint generation method." Operations Research Letters **41**(5): 457-461.

Zhang, C., X. Liu, Y. Jiang, B. Fan and X. Song (2016). "A two-stage resource allocation model for lifeline systems quick response with vulnerability analysis." European Journal of Operational Research **250**(3): 855-864.

Zhao, L. and B. Zeng (2012). "An exact algorithm for two-stage robust optimization with mixed integer recourse problems." submitted, available on Optimization-Online. org.

Zio, E. (2016). "Challenges in the vulnerability and risk analysis of critical infrastructures." Reliability Engineering & System Safety **152**: 137-150.

Zio, E. and G. Sansavini (2011). "Modeling interdependent network systems for identifying cascade-safe operating margins." IEEE Transactions on Reliability **60**(1): 94-101.